

Semivariogram methods for modeling Whittle-Matérn priors in Bayesian inverse problems

R D Brown¹, Johnathan M Bardsley¹ and Tiangang Cui²

¹ Department of Mathematical Sciences, University of Montana, Missoula, MT 59812

² Department of Mathematics, Monash University, Melbourne, Australia

E-mail: rick.brown@umontana.edu, bardsleyj@mso.umt.edu,
Tiangang.Cui@monash.edu

Abstract. We present a new technique, based on semivariogram methodology, for obtaining point estimates for use in prior modeling for solving Bayesian inverse problems. This method requires a connection between Gaussian processes with covariance operators defined by the Matérn covariance function and Gaussian processes with precision (inverse-covariance) operators defined by the Green’s functions of a class of elliptic stochastic partial differential equations (SPDEs). We present a detailed mathematical description of this connection. We will show that there is an equivalence between these two Gaussian processes when the domain is infinite – for us, \mathbb{R}^2 – which breaks down when the domain is finite due to the effect of boundary conditions on Green’s functions of PDEs. We show how this connection can be re-established using extended domains. We then introduce the semivariogram method for estimating the Matérn covariance parameters, which specify the Gaussian prior needed for stabilizing the inverse problem. Results are extended from the isotropic case to the anisotropic case where the correlation length in one direction is larger than another. Finally, we consider the situation where the correlation length is spatially dependent rather than constant. We implement each method in two-dimensional image inpainting test cases to show that it works on practical examples.

Keywords: inverse problems, variogram, Bayesian methods, boundary conditions, Whittle-Matérn, stochastic partial differential equations, Gaussian field

1. Introduction

Inverse problems are ubiquitous in science and engineering. They are characterized by the estimation of parameters in a mathematical model from measurements and by a high-dimensional parameter space that typically results from discretizing a function defined on a computational domain. For typical inverse problems, the process of estimating model parameters from measurements is ill-posed, which motivates the use of regularization in the deterministic setting and the choice of a prior probability density in the Bayesian setting. In this paper, we consider linear models of the form

$$\mathbf{b} = \mathbf{A}\mathbf{x} + \boldsymbol{\epsilon}, \quad \boldsymbol{\epsilon} \sim \mathcal{N}(\mathbf{0}, \lambda^{-1}\mathbf{I}_M), \quad (1)$$

where $\mathbf{b} \in \mathbb{R}^M$ is the vector of measurements, $\mathbf{A} \in \mathbb{R}^{M \times N}$ is the forward model matrix, $\mathbf{x} \in \mathbb{R}^N$ is the vector of unknown parameters, and $\boldsymbol{\epsilon} \sim \mathcal{N}(\mathbf{0}, \lambda^{-1} \mathbf{I}_M)$ is the observation noise that follows a zero-mean Gaussian distribution with covariance matrix $\lambda^{-1} \mathbf{I}_M$, with \mathbf{I}_M denoting the $M \times M$ identity. In typical inverse problems, $\mathbf{A}\mathbf{x}$ is the discretization of a continuous forward model Ax , where A is a linear operator and x is a function. The components of the vector \mathbf{x} satisfy $x_i = x(\mathbf{u}_i)$, where $\mathbf{u}_i \in \mathbb{R}^d$ is the location of the i th element of the numerical grid. The random vector \mathbf{b} in (1) has conditional probability density function

$$p(\mathbf{b}|\mathbf{x}, \lambda) \propto \exp\left(-\frac{\lambda}{2} \|\mathbf{A}\mathbf{x} - \mathbf{b}\|^2\right), \quad (2)$$

where \propto denotes proportionality and $\|\cdot\|$ denotes the ℓ^2 -norm. The maximizer of $p(\mathbf{b}|\mathbf{x}, \lambda)$ with respect to \mathbf{x} is known as the maximum likelihood estimator, and we denote it by \mathbf{x}_{ML} . As stated above, due to ill-posedness, \mathbf{x}_{ML} is unstable with respect to errors in \mathbf{b} , i.e., small changes in \mathbf{b} result in large relative changes in \mathbf{x}_{ML} .

There are various methods to stabilize the solution of inverse problems, but they all involve some form of regularization. In this paper, we take the Bayesian approach [1], which requires the definition of a prior probability density function on \mathbf{x} . We make the assumption that the prior is Gaussian of the form $\mathbf{x} \sim \mathcal{N}(\mathbf{0}, (\delta \mathbf{P})^{-1})$, which has probability density function

$$p(\mathbf{x}|\delta) \propto \exp\left(-\frac{\delta}{2} \mathbf{x}^T \mathbf{P} \mathbf{x}\right), \quad (3)$$

where \mathbf{P} is the precision (inverse-covariance) matrix.

Now that we have defined the prior (3) and the likelihood (2), using Bayes' law, we multiply them together to obtain the posterior density function

$$\begin{aligned} p(\mathbf{x}|\mathbf{b}, \lambda, \delta) &\propto p(\mathbf{b}|\mathbf{x}, \lambda) p(\mathbf{x}|\delta) \\ &\propto \exp\left(-\frac{\lambda}{2} \|\mathbf{A}\mathbf{x} - \mathbf{b}\|^2 - \frac{\delta}{2} \mathbf{x}^T \mathbf{P} \mathbf{x}\right), \end{aligned} \quad (4)$$

whose maximizer, $\mathbf{x}_{\lambda, \delta}$, is known as the maximum a posteriori (MAP) estimator. The MAP estimator can be equivalently expressed as

$$\mathbf{x}_{\lambda, \delta} = \arg \min_{\mathbf{x}} \left\{ \frac{\lambda}{2} \|\mathbf{A}\mathbf{x} - \mathbf{b}\|^2 + \frac{\delta}{2} \mathbf{x}^T \mathbf{P} \mathbf{x} \right\}.$$

Our primary focus in this paper is to provide formulations and parameter selection techniques for prior precision matrices that have an intuitive interpretation and can be used to solve a wide variety of problems.

1.1. The Matérn Class of Covariance Matrices and Whittle-Matérn Priors

It remains to define the prior covariance matrix $\mathbf{C} = \mathbf{P}^{-1}$. The Matérn class of covariance matrices has garnered much praise [2] for its flexibility in capturing many covariance structures and its allowance of direct control of the degree of correlation in

the vector \mathbf{x} [3]. The Matérn covariance matrix is defined by the Matérn covariance function, which was first formulated by Matérn in 1947 [4],

$$C(r) = \sigma^2 \frac{(r/\ell)^\nu K_\nu(r/\ell)}{2^{\nu-1} \Gamma(\nu)}, \quad (5)$$

where r is the separation distance; $K_\nu(\cdot)$ is the modified Bessel function of the second kind of order ν [5]; $\Gamma(\cdot)$ is the gamma function; $\ell > 0$ is the range parameter; $\nu > 0$ is the smoothness parameter; and σ^2 is the marginal variance. Omitting σ^2 gives the Matérn correlation function. In the isotropic case, when the covariance depends only on the distance between elements, given the covariance parameters σ^2, ν , and ℓ , one can obtain the covariance matrix \mathbf{C} of a vector $\mathbf{x} = [x_1, \dots, x_N]^T$ with spatial positions $\{\mathbf{u}_1^T, \dots, \mathbf{u}_N^T\} \subset \mathbb{R}^d$ by letting

$$[\mathbf{C}]_{ij} = \text{Cov}(x_i, x_j) = C(\|\mathbf{u}_i - \mathbf{u}_j\|),$$

where C is defined by (5).

The parameters of the Matérn covariance function are not as straightforward to interpret as the parameters of some other covariance functions. When ν is small ($\nu \rightarrow 0^+$), the spatial process is said to be rough, and when it is large ($\nu \rightarrow \infty$), the process is smooth [3, 6]. Figure 1 shows how the covariance function behaves with different values of ℓ and ν : on the left, $\ell = \sigma^2 = 1$ and ν varies, while on the right $\nu = \sigma^2 = 1$ and ℓ varies. Note that as ν increases, the behavior at small lags changes, leading to more correlation at smaller distances and a larger *practical range*, which is defined to be the distance at which the correlation is equal to 0.05. In Figure 1, this is the distance at which the covariance function intersects the horizontal line. Meanwhile, as ℓ decreases, the decay rate of the covariance increases considerably, which decreases the practical range. Although ℓ is known as the range parameter, the parameter ν also affects the practical range. In [7], a range approximation $\rho = \ell\sqrt{8\nu}$ is used where $C(\rho) \approx 0.10$.

Despite the benefits of using the Matérn class of covariance matrices, its use can be problematic for inverse problems because computing the precision matrix \mathbf{P} , which is what appears in the posterior (4), requires inverting a dense $N \times N$ matrix. Using the fast Fourier transform (FFT) [8, 9, 10] to operate with \mathbf{P} and \mathbf{C} more efficiently is recommended if \mathbf{x} is defined on a regular grid and periodic boundary conditions are assumed. In other cases, it is useful that the Matérn covariance function has a direct connection to a class of elliptic SPDEs [7] whose numerical discretization yields sparse precision matrices, \mathbf{P} , that are computationally feasible to work with even when N is large. Connections of this type were first shown to exist by Whittle in [11], where he showed the connection held for a special case of the Matérn covariance class. Hence, priors that depend on this connection are often referred to as Whittle-Matérn priors. The connection between the general Matérn covariance function and SPDEs has been used in a wide range of applications for defining computationally feasible priors for high-dimensional problems [12, 13, 14]. Moreover, work has been done in establishing

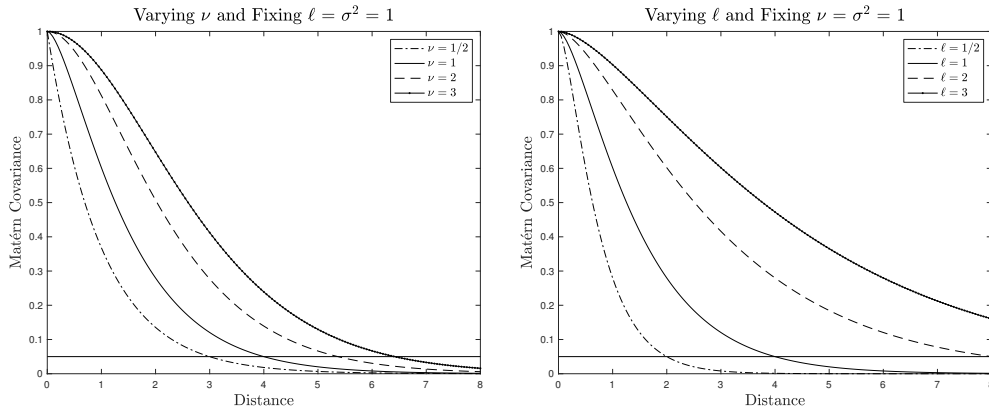


Figure 1. Behavior of the Matérn covariance function. The smoothness parameter, ν , primarily affects the covariance at small distances whereas the range parameter, ℓ , mainly affects the decay rate of the covariance. The horizontal line corresponds to a covariance value of 0.05 and the practical range is the distance at which the covariance intersects this line.

convergence theorems for, and lattice approximations of, these Whittle-Matérn priors [15].

The remainder of the paper is organized as follows. In Section 2, we describe in detail the connection between zero-mean Gaussian processes with the isotropic Matérn covariance operator and those that arise as solutions of a class of elliptic SPDEs. In Section 3, we show how to estimate the parameters in the isotropic Whittle-Matérn prior using the semivariogram method, and then we show how to use this approach to define the prior when solving a Bayesian inverse problem. In Section 4, we extend these ideas to the anisotropic case and then we consider images with regions that require different covariance structures in Section 5. For each section, we present numerical tests on two-dimensional image inpainting test cases. We end with conclusions in Section 6.

2. Whittle-Matérn Class Priors via SPDEs

In this section, we will show that the Whittle-Matérn class of priors can be specified as the solution of the SPDE

$$(1 - \ell^2 \Delta)^{\beta/2} x(\mathbf{u}) = \mathcal{W}(\mathbf{u}), \quad \mathbf{u} \in \mathbb{R}^d, \quad \beta = \nu + d/2, \quad \ell, \nu > 0, \quad (6)$$

where $\Delta = \sum_{i=1}^d \frac{\partial^2}{\partial u_i^2}$ is the Laplacian operator in d dimensions, and \mathcal{W} is spatial Gaussian white noise with unit variance, which we define below. Although this connection has been shown to exist [11, 7, 13], here we provide a significantly more detailed derivation of this result than we have seen elsewhere. This derivation also provides a viable way to construct other Gaussian processes using differential operators.

2.1. Preliminary Definitions

Before deriving the solution of (6), we need some preliminary definitions.

2.1.1. Gaussian Fields A stochastic process $\{x(\mathbf{u}), \mathbf{u} \in \Omega\}$, with $\Omega \subset \mathbb{R}^d$, is a *Gaussian field* [16] if for any $k \geq 1$ and any locations $\mathbf{u}_1, \dots, \mathbf{u}_k \in \Omega$, $[x(\mathbf{u}_1), \dots, x(\mathbf{u}_k)]^T$ is a normally distributed random vector with mean $\boldsymbol{\mu} = [E[x(\mathbf{u}_1)], \dots, E[x(\mathbf{u}_k)]]^T$, where $E[\cdot]$ denotes expected value, and covariance matrix $[\mathbf{C}]_{ij} = \text{Cov}(x(\mathbf{u}_i), x(\mathbf{u}_j)) = E[(x(\mathbf{u}_i) - E[x(\mathbf{u}_i)])(x(\mathbf{u}_j) - E[x(\mathbf{u}_j)])]$, for $1 \leq i, j \leq k$. The covariance function is defined $C(\mathbf{u}_i, \mathbf{u}_j) := \text{Cov}(x(\mathbf{u}_i), x(\mathbf{u}_j))$. It is necessary that the covariance function is positive definite, i.e., for any $\{\mathbf{u}_1, \dots, \mathbf{u}_k\}$, with $k \geq 1$, the covariance matrix \mathbf{C} defined above is positive definite. The Gaussian field is called *stationary* if the mean is constant and the covariance function satisfies $C(\mathbf{u}, \mathbf{v}) = C(\mathbf{u} - \mathbf{v})$ and *isotropic* if $C(\mathbf{u}, \mathbf{v}) = C(\|\mathbf{u} - \mathbf{v}\|)$.

2.1.2. White Noise The term *white noise* [17, 18] comes from light. White light is a homogeneous mix of wavelengths, as opposed to colored light, which is a heterogeneous mix of wavelengths. In a similar way, white noise contains a homogeneous mix of all the different basis functions. The mixing of these basis functions is determined by a random process. When this random process is Gaussian, we have *Gaussian white noise*. Consider a domain Ω and let $\{\phi_j : j = 1, 2, \dots\}$ be an orthonormal basis of $L^2(\Omega)$ where $L^2(\Omega) = \{f : \Omega \rightarrow \mathbb{R} \mid \int_{\Omega} |f(x)|^2 dx < \infty\}$. Then Gaussian white noise is defined by

$$\mathcal{W}(\mathbf{u}) = \sum_{j=1}^{\infty} \xi_j \phi_j(\mathbf{u}), \quad \xi_j \stackrel{iid}{\sim} \mathcal{N}(0, \eta^2). \quad (7)$$

If we are dealing with spatial Gaussian white noise with unit variance, then \mathbf{u} refers to location and if $\eta^2 = 1$. With this definition, it is clear that Gaussian white noise has mean zero: $E[\mathcal{W}(\mathbf{u})] = \sum_{j=1}^{\infty} E[\xi_j] \phi_j(\mathbf{u}) = 0$. Moreover, one can show that $\text{Cov}(\mathcal{W}(\mathbf{u}), \mathcal{W}(\mathbf{v})) = \eta^2 \delta(\mathbf{u} - \mathbf{v})$, where $\delta(\cdot)$ is the *Dirac delta function* [19], also known as the delta distribution. A well-known and very important property of the Dirac delta function is that it satisfies the *sifting property*: $f(\mathbf{u}) = \int_{-\infty}^{\infty} \delta(\mathbf{u} - \mathbf{v}) f(\mathbf{v}) d\mathbf{v}$.

2.1.3. Green's Functions We now consider differential equations of the form $Lx(\mathbf{u}) = f(\mathbf{u})$, $\mathbf{u} \in \mathbb{R}^d$, where L is a linear, differential operator. A *Green's function* [20, 21], g , of L is any solution of $Lg(\mathbf{u}, \mathbf{v}) = \delta(\mathbf{u} - \mathbf{v})$, where $\delta(\cdot)$ is the Dirac delta function. Using the Green's function, the solution of the equation $Lx(\mathbf{u}) = f(\mathbf{u})$ can be written as

$$x(\mathbf{u}) = \int_{\mathbb{R}^d} g(\mathbf{u}, \mathbf{v}) f(\mathbf{v}) d\mathbf{v}. \quad (8)$$

2.2. The Gaussian Field Solution of the SPDE (6)

In this subsection, we will prove the following theorem concerning the solution of the SPDE (6).

Theorem 1 *The solution $x(\mathbf{u})$ of (6) is a Gaussian field with mean zero and Matérn covariance function defined by (5).*

Proof. To begin, we note that the Green's function for (6) is the solution of

$$(1 - \ell^2 \Delta)^{\beta/2} g(\mathbf{u}, \mathbf{v}) = \delta(\mathbf{v} - \mathbf{u}). \quad (9)$$

Using (8), the solution to (6) is given by

$$x(\mathbf{u}) = \int_{\mathbb{R}^d} g(\mathbf{u}, \mathbf{v}) \mathcal{W}(\mathbf{v}) d\mathbf{v}, \quad (10)$$

making $x(\mathbf{u})$ a Gaussian field since it is a linear transformation of Gaussian white noise.

We now compute the mean and covariance of the Gaussian field, $x(\mathbf{u})$, defined by (10). Since the Green's function is a strictly-positive, symmetric, and rapidly decaying function, we can apply Fubini's theorem [22] to obtain the mean of $x(\mathbf{u})$:

$$E[x(\mathbf{u})] = E \left[\int_{\mathbb{R}^d} g(\mathbf{u}, \mathbf{v}) \mathcal{W}(\mathbf{v}) d\mathbf{v} \right] = \int_{\mathbb{R}^d} g(\mathbf{u}, \mathbf{v}) E[\mathcal{W}(\mathbf{v})] d\mathbf{v} = 0.$$

Since $x(\mathbf{u})$ has mean zero, the covariance is given by

$$\begin{aligned} \text{Cov}(x(\mathbf{u}), x(\mathbf{u}')) &= E[x(\mathbf{u})x(\mathbf{u}')] \\ &= \int_{\mathbb{R}^d} \left(\int_{\mathbb{R}^d} E[\mathcal{W}(\mathbf{v})\mathcal{W}(\mathbf{v}')] g(\mathbf{u}, \mathbf{v}) d\mathbf{v} \right) g(\mathbf{u}', \mathbf{v}') d\mathbf{v}' \\ &= \int_{\mathbb{R}^d} \left(\int_{\mathbb{R}^d} \delta(\mathbf{v} - \mathbf{v}') g(\mathbf{u}, \mathbf{v}) d\mathbf{v} \right) g(\mathbf{u}', \mathbf{v}') d\mathbf{v}' \\ &= \int_{\mathbb{R}^d} g(\mathbf{u}, \mathbf{v}') g(\mathbf{u}', \mathbf{v}') d\mathbf{v}'. \end{aligned}$$

If we define $C(\mathbf{u}, \mathbf{u}') := \text{Cov}(x(\mathbf{u}), x(\mathbf{u}'))$, the previous result implies that if $L = (1 - \ell^2 \Delta)^{\beta/2}$, then for our linear L acting only on \mathbf{u}' ,

$$\begin{aligned} LC(\mathbf{u}, \mathbf{u}') &= L \int_{\mathbb{R}^d} g(\mathbf{u}, \mathbf{v}') g(\mathbf{u}', \mathbf{v}') d\mathbf{v}' \\ &= \int_{\mathbb{R}^d} [Lg(\mathbf{u}', \mathbf{v}')] g(\mathbf{u}, \mathbf{v}') d\mathbf{v}' \\ &= \int_{\mathbb{R}^d} \delta(\mathbf{u}' - \mathbf{v}') g(\mathbf{u}, \mathbf{v}') d\mathbf{v}' \\ &= g(\mathbf{u}, \mathbf{u}'). \end{aligned} \quad (11)$$

To derive the Green's function g in (11), we first define $g(\mathbf{u}) := g(\mathbf{u}, \mathbf{0})$. Then (9) implies

$$(1 - \ell^2 \Delta)^{\beta/2} g(\mathbf{u}) = \delta(\mathbf{u}). \quad (12)$$

To proceed, we must take the Fourier transform [23, 24] of both sides of (12). This yields

$$(1 + \ell^2 \|\boldsymbol{\omega}\|^2)^{\beta/2} \hat{g}(\boldsymbol{\omega}) = 1,$$

where $\boldsymbol{\omega} \in \mathbb{C}^d$ are the coordinates in the Fourier-transformed space and the hat (\hat{f}) notation denotes the Fourier-transform of a function f . Thus, the Fourier transform of the Green's function is

$$\hat{g}(\boldsymbol{\omega}) = (1 + \ell^2 \|\boldsymbol{\omega}\|^2)^{-\beta/2}. \quad (13)$$

Next, we assume *stationarity* so that the covariance only depends on the relative locations of the points, i.e., $\mathbf{r} := \mathbf{u} - \mathbf{v}$. Then $E[x(\mathbf{u})x(\mathbf{v})] = E[x(\mathbf{r})x(\mathbf{0})] = C(\mathbf{r}, \mathbf{0}) := C(\mathbf{r})$ and (11) can be expressed $LC(\mathbf{r}) = g(\mathbf{r})$. If we take the Fourier transform of both sides of this equation, and appeal to (13), we obtain

$$\hat{C}(\boldsymbol{\omega}) = (1 + \ell^2 \|\boldsymbol{\omega}\|^2)^{-\beta}.$$

Since the Laplacian, Δ , is invariant under rotations and translations, we have radial symmetry, which is analogous to isotropy in the covariance. Thus we can let $s = \|\boldsymbol{\omega}\|$ and $r = \|\mathbf{r}\|$ to obtain the equivalent expression

$$\hat{C}(s) = (1 + \ell^2 s^2)^{-\beta}. \quad (14)$$

To transform back to the original (r) space, we use the Hankel transform [25] and its relationship to the radially symmetric Fourier transform, i.e.,

$$s^{\frac{d-2}{2}} \hat{C}(s) = (2\pi)^{\frac{d}{2}} \int_0^\infty J_{\frac{d-2}{2}}(sr) r^{\frac{d-2}{2}} C(r) r dr,$$

where C is the original (untransformed) covariance function and $J_\nu(\cdot)$ is the Bessel function of the first kind of order ν ; see [26, Section 2] for a proof. Using appropriate substitutions in the inverse Hankel transform and (14), we obtain

$$C(r) = \frac{(2\pi)^{-\frac{d}{2}}}{r^{\frac{d-1}{2}}} \int_0^\infty J_{\frac{d-2}{2}}(sr) s^{\frac{d-1}{2}} (1 + \ell^2 s^2)^{-\beta} (sr)^{1/2} ds.$$

Finally, using the integral identity [27, Eq. 20, p. 24, vol. II] and some algebra, we obtain

$$C(r) = \frac{\ell^{-\frac{d}{2}} r^{\beta - \frac{d}{2}} K_{\frac{d}{2} - \beta}(r/\ell)}{(2\pi)^{\frac{d}{2}} 2^{\beta-1} \Gamma(\beta)}. \quad (15)$$

Using the fact that $K_\nu = K_{-\nu}$, and defining $\sigma^2 := \ell^{\nu+d/2} \Gamma(\nu) [(4\pi)^{d/2} \Gamma(\nu + d/2)]^{-1}$ with $\nu := \beta - d/2$, it can be shown that (15) is exactly the Matérn covariance function (5). \square

2.3. The Effect of a Finite Domain and Boundary Conditions

The proof of Theorem 1 above assumed that the domain was all of \mathbb{R}^d , i.e. $\Omega = \mathbb{R}^d$. However, when solving inverse problems, $x(\mathbf{u})$ is restricted to a finite domain $\Omega \subset \mathbb{R}^d$. In such cases, boundary conditions that modify the Green's function must be assumed, and thus the equivalence between the Gaussian fields defined by the SPDE (6) and those defined by the Matérn covariance function may not hold.

To see this, consider the case where $d = 2$ and $\Omega = [0, 1] \times [0, 1]$ with Dirichlet (zero) boundary conditions, $x(0, t) = x(1, t) = x(s, 0) = x(s, 1) = 0$, where $0 \leq s, t \leq 1$. Additionally, we assume $\nu = 1$ so that the exponent of the differential operator is equal to one, making the discretization straightforward. In this case, (6) simplifies to

$$(1 - \ell^2 \Delta)x(\mathbf{u}) = \mathcal{W}(\mathbf{u}), \quad \mathbf{u} \in \mathbb{R}^2, \quad \ell > 0.$$

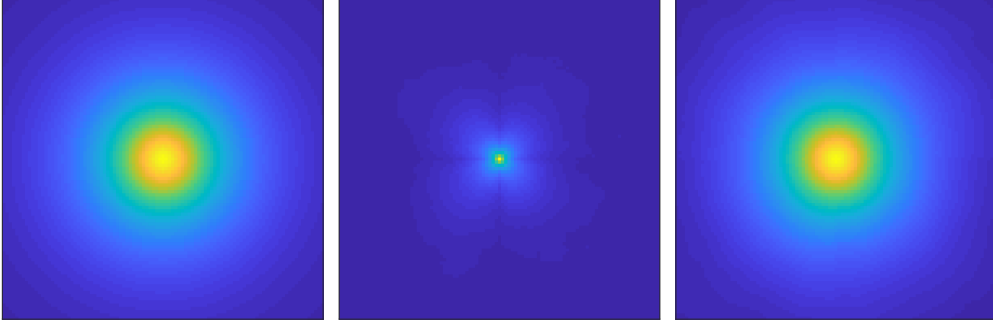


Figure 2. Isotropic correlation maps. Plots of the Matérn correlation map (left), the empirical correlation map with $n = 50$ computed on the domain $\Omega = [0, 1] \times [0, 1]$ (middle), and the empirical correlation map computed on the domain $\bar{\Omega} = [-0.5, 1.5] \times [-0.5, 1.5]$ (right), computed from random draws from the prior (16) in 2D with $\nu = 1$ and $\ell = 1/4$.

Using a uniform mesh on $[0, 1] \times [0, 1]$ with a step size of $h = 1/n$, so that $N = n^2$, yields the numerical discretization

$$(\mathbf{I}_N + (\ell/h)^2 \mathbf{L}_{2D}) \mathbf{x} = \delta^{-1/2} \boldsymbol{\xi}, \quad \boldsymbol{\xi} \sim \mathcal{N}(\mathbf{0}, \mathbf{I}_n),$$

where δ is the scaling parameter for the prior and $(1/h^2) \mathbf{L}_{2D} \mathbf{x}$ is the standard finite-difference discretization of $(-\partial^2 x(\mathbf{u})/\partial u_1^2 - \partial^2 x(\mathbf{u})/\partial u_2^2)$ [10]. Then the probability density for \mathbf{x} is given by

$$\mathbf{x} | \delta, \ell \sim \mathcal{N}(\mathbf{0}, \delta^{-1} (\mathbf{I} + (\ell/h)^2 \mathbf{L}_{2D})^{-2}),$$

or equivalently,

$$p(\mathbf{x} | \delta, \ell) \propto \exp\left(-\frac{\delta}{2} \mathbf{x}^T (\mathbf{I} + (\ell/h)^2 \mathbf{L}_{2D})^2 \mathbf{x}\right). \quad (16)$$

We now let $n = 50$, so $N = 50^2 = 2500$, and generate 50 000 samples from (16) for each of N x_i values, calculate the empirical correlation between the samples, and compare this with the theoretical correlation defined by the Matérn covariance function. We do this for $\ell = 1/4$ and plot the results in the middle of Figure 2, together with the Matérn correlation map on the left. It is clear that there is a disconnection between the empirical covariance and the Matérn covariance.

It is crucial that the connection between the Gaussian fields defined by the SPDE and those defined by the Matérn covariance function holds because then the parameters in the SPDE can be estimated using the semivariogram method described in Section 3. Fortunately, we can restore this connection by extending the computational domain. In two dimensions, we define $\bar{\Omega} = [1 - a, a] \times [1 - a, a]$, for $a > 1$, e.g., if $a = 1.5$ then $\bar{\Omega} = [-0.5, 1.5] \times [-0.5, 1.5]$. We then generate realizations for $((2a - 1)n)^2 = (2n)^2 = 10\,000$ x_i values on the extended domain and compute the empirical correlation only for the x_i values that correspond to the original domain, $\Omega = [0, 1] \times [0, 1]$. The results are plotted on the right side of Figure 2, where it is clear that the empirical correlation map is nearly indistinguishable from those obtained using the Matérn correlation function.

To determine the a value that extends the domain far enough to restore the Matérn/SPDE connection, but not so far as to introduce unnecessary computational cost, we look to the Matérn correlation function itself. We want to extend the domain far enough so that all \mathbf{x} values in $[0, 1] \times [0, 1]$ have a sufficiently low correlation with the \mathbf{x} values at the end of the extended domain. In tests, it was found that we should always extend the domain at least slightly. If we let r_c be the distance for which the Matérn correlation is approximately equal to c , then our tests showed that setting $a = 1 + r_{0.40}$ restores the connection to the Matérn covariance for $\nu \geq 1/2$ when using zero boundary conditions and setting $a = 1 + r_{0.30}$ restores the connection to the Matérn covariance for $\nu \geq 1/2$ when periodic boundary conditions are used. For $\nu = 1$ and $\ell = 1/4$, a should be set to 1.4 in the Dirichlet boundary condition case and 1.5 when using periodic boundary conditions. We note that since ℓ is directly related to the degree of correlation in the prior, the extension necessary to preserve the connection rises sharply as ℓ increases. It is rare in practice, however, to have $\ell > 1/4$ when $\nu \geq 1$ since that implies the correlation persists across the entire region. Thus, it is uncommon to have to extend beyond a domain of $[-0.5, 1.5] \times [-0.5, 1.5]$.

For the above discussion, we focused on zero boundary conditions. Similar results hold if periodic boundary conditions are assumed, in which case \mathbf{L} , and thus \mathbf{L}_{2D} , can be diagonalized by the FFT, assuming \mathbf{x} is defined on a regular grid. The FFT-based diagonalization of \mathbf{L}_{2D} can be exploited to greatly reduce computational cost, thus when extending the domain in two-dimensions, it is advantageous to use periodic boundary conditions and the extended domain $\bar{\Omega} = [-0.5, 1.5] \times [-0.5, 1.5]$ so that \mathbf{L}_{2D} defined on $\bar{\Omega}$ can be diagonalized by the FFT. A more thorough description of the effects of boundary artifacts with different boundary conditions can be found in [28].

Finally, in our numerical experiment above, we chose specific values of ν , but other values of ν can be chosen. The general form of the isotropic prior density in two dimensions, with ν included as a parameter, is

$$p(\mathbf{x}|\delta, \nu, \ell) \propto \exp\left(-\frac{\delta}{2}\mathbf{x}^T(\mathbf{I} + (\ell/h)^2\mathbf{L}_{2D})^{\nu+d/2}\mathbf{x}\right). \quad (17)$$

If $\nu + d/2$ is a non-integer, a fractional power of $\mathbf{I} + (\ell/h)^2\mathbf{L}_{2D}$ must be computed, which is possible, generally speaking, if we have a diagonalization of $\mathbf{I} + (\ell/h)^2\mathbf{L}_{2D}$ in hand, but the resulting precision matrix is not sparse. Such a diagonalization is typically computable in one-dimensional examples, even with dense matrices. In two dimensions, however, an efficient diagonalization is possible only if periodic boundary conditions are assumed. We will restrict the exponent $\nu + d/2$ to be an integer in this paper to preserve the sparsity in the precision matrix, which will be especially useful in Section 5.

2.4. Computing MAP Estimators for Whittle-Matérn Priors

Using Bayes' law, we multiply the prior (17) by the likelihood (2) to obtain the posterior density function

$$p(\mathbf{x}|\mathbf{b}, \lambda, \delta, \nu, \ell) \propto p(\mathbf{b}|\mathbf{x}, \lambda)p(\mathbf{x}|\delta, \nu, \ell)$$

$$\propto \exp\left(-\frac{\lambda}{2}\|\mathbf{A}\mathbf{x} - \mathbf{b}\|^2 - \frac{\delta}{2}\mathbf{x}^T(\mathbf{I} + (\ell/h)^2\mathbf{L}_{2D})^{\nu+d/2}\mathbf{x}\right).$$

The maximizer of $p(\mathbf{x}|\mathbf{b}, \lambda, \delta, \nu, \ell)$ is known as the MAP estimator, and it can be computed by solving

$$\begin{aligned}\mathbf{x}_\alpha &= \arg \min_{\mathbf{x}} \left\{ \frac{1}{2}\|\mathbf{A}\mathbf{x} - \mathbf{b}\|^2 + \frac{\alpha}{2}\mathbf{x}^T(\mathbf{I} + (\ell/h)^2\mathbf{L}_{2D})^{\nu+d/2}\mathbf{x} \right\} \\ &= (\mathbf{A}^T\mathbf{A} + \alpha(\mathbf{I} + (\ell/h)^2\mathbf{L}_{2D})^{\nu+d/2})^{-1}\mathbf{A}^T\mathbf{b},\end{aligned}\tag{18}$$

where $\alpha = \delta/\lambda$. Assuming we know ℓ and ν , α can be estimated using one of many regularization parameter selection methods (see, e.g., [29, 30, 10]). One such method is generalized cross validation (GCV):

$$\alpha = \arg \min_{\eta > 0} \left\{ \frac{\left\| \mathbf{A}(\mathbf{A}^T\mathbf{A} + \eta\mathbf{P})^{-1}\mathbf{A}^T\mathbf{b} - \mathbf{b} \right\|^2}{\text{tr}\left(\mathbf{I} - \mathbf{A}(\mathbf{A}^T\mathbf{A} + \eta\mathbf{P})^{-1}\mathbf{A}^T\right)} \right\}\tag{19}$$

for $\mathbf{P} = (\mathbf{I} + (\ell/h)^2\mathbf{L}_{2D})^{\nu+d/2}$.

In practice, ν is often fixed [31, 12] and ℓ is either estimated manually or by using the fully Bayesian approach, which involves Markov chain Monte Carlo (MCMC) [32] sampling. This requires setting up hyper-prior distributions and can be time consuming, subjective and unintuitive, so we present a new method for selecting these parameters next.

3. The Semivariogram Method for Estimating ν and ℓ

In the inverse problem formulation above, the components of the vector \mathbf{x} correspond to values of an unknown function x at numerical mesh points within a spatial region Ω . This motivates using methods from spatial statistics to estimate the Whittle-Matérn prior parameters ν and ℓ . One such method uses a variogram, and a corresponding semivariogram [33], which requires the assumption of *intrinsic stationarity*, i.e., that the elements of \mathbf{x} have constant mean and the variance of the difference between the elements is constant throughout the region. This is a weaker assumption than is required by many other parameter estimation tools, which is one of the reasons variograms have become popular in spatial statistical applications [34], and it is the reason we use semivariograms here. Although the use of semivariograms for estimating parameters to determine a covariance structure is commonly used in spatial statistics, this is, to our knowledge, the first time these tools have been used to estimate prior parameters for use in inverse problems.

The semivariogram is defined by $\gamma(\mathbf{r}) = \frac{1}{2}\text{Var}[X(\mathbf{u}_i) - X(\mathbf{u}_j)]$, where $\mathbf{r} = \mathbf{u}_i - \mathbf{u}_j$ and $\{X(\mathbf{u}) : \mathbf{u} \in \Omega \subset \mathbb{R}^d\}$ is a spatial process. Due to our stationarity assumption, $\text{Var}[X(\mathbf{u}_i)] = \text{Var}[X(\mathbf{u}_j)] = \sigma^2$, which we use to derive the following alternative

expression for $\gamma(\mathbf{r})$:

$$\begin{aligned}\gamma(\mathbf{r}) &= \frac{1}{2} \left(\text{Var}[X(\mathbf{u}_i)] + \text{Var}[X(\mathbf{u}_j)] - 2\text{Cov}[X(\mathbf{u}_i), X(\mathbf{u}_j)] \right) \\ &= \sigma^2 - \text{Cov}[X(\mathbf{u}_i), X(\mathbf{u}_j)].\end{aligned}$$

Thus, the semivariogram simplifies to the difference between the variance in the region and the covariance between two points with a difference \mathbf{r} . The variogram is formally defined as $2\gamma(\mathbf{r})$, hence the terms variogram and semivariogram are often used interchangeably. To remain consistent, we will continue to refer to $\gamma(\mathbf{r})$ as a semivariogram throughout the paper.

We now need a way to estimate the semivariogram from given data. For this, we use what is known as the sample, or empirical, semivariogram. Assuming that $X(\mathbf{u})$ is isotropic, so that $r = \|\mathbf{r}\| = \|\mathbf{u}_i - \mathbf{u}_j\|$, then the empirical semivariogram can be expressed

$$\hat{\gamma}(r) = \frac{1}{2n(r)} \sum_{(i,j) \|\mathbf{u}_i - \mathbf{u}_j\|=r} [x(\mathbf{u}_i) - x(\mathbf{u}_j)]^2, \quad (20)$$

where $x(\mathbf{u})$ is a realization of $X(\mathbf{u})$, and $n(r)$ is the number of points that are separated by a distance r . The $\hat{\gamma}(r)$ values are often referred to as the semivariance values. In a typical semivariogram, the semivariance values increase as r increases since points tend to be less similar the further apart they are, which increases the variance of their differences.

Although the empirical semivariogram is useful in obtaining semivariance values from data, it is not ideal for modeling data for various reasons (see [34] for details), thus it is typical to fit a semivariogram model to the empirical semivariogram. Since our prior distribution for \mathbf{x} has a Matérn covariance, we will use the theoretical Matérn semivariogram model [4, 2] given by

$$\gamma(r, \boldsymbol{\theta}) = \begin{cases} 0 & \text{if } r = 0 \\ a_0 + (\sigma^2 - a_0) \left[1 - \frac{1}{2^{\nu-1}\Gamma(\nu)} (r/\ell)^\nu K_\nu(r/\ell) \right] & \text{if } r > 0 \end{cases} \quad (21)$$

where $a_0 \geq 0$ is the nugget, $\sigma^2 \geq a_0$ is the sill, and $\boldsymbol{\theta} = (a_0, \sigma^2, \nu, \ell)$. The nugget is the term given to the semivariance value at a distance just greater than zero and the sill is the total variance contribution or the semivariance value where the model levels out. The sill, σ^2 , is also the variance parameter in the Matérn covariance function (5). We can estimate a_0 , σ^2 , ν , and ℓ by fitting the semivariogram model to the empirical semivariogram.

There are a number of ways to fit the semivariogram model to the empirical semivariogram. We use weighted least squares, as is commonly done [34], choosing the $\boldsymbol{\theta}$ that minimizes

$$W(\boldsymbol{\theta}) = \sum_r \frac{n(r)}{2[\gamma(r, \boldsymbol{\theta})]^2} [\hat{\gamma}(r) - \gamma(r, \boldsymbol{\theta})]^2. \quad (22)$$

To minimize $W(\boldsymbol{\theta})$, we adapt the MATLAB codes from [35, 36]. More specifically, we adapt [35] for computing the empirical semivariance $\hat{\gamma}(r)$ and we adapt [36] for

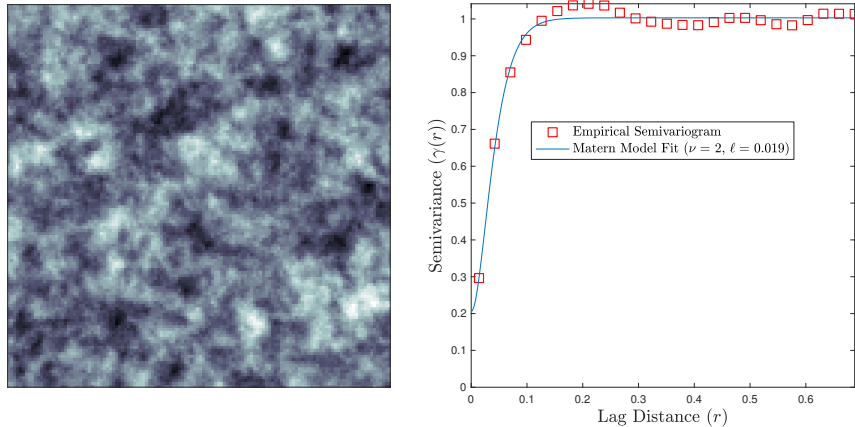


Figure 3. Semivariogram. A randomly generated spatial field is shown on the left and the empirical semivariogram, along with the Matérn model fit, is given on the right. The fitted parameters are $\nu = 2$ and $\ell = 0.019$, which corresponds to a practical range of 0.102.

minimizing $W(\boldsymbol{\theta})$. Although it is possible to optimize both ν and ℓ continuously, we will require $\nu + d/2$ to be an integer.

For an illustration, we generated a random field, shown on the left side of Figure 3, and fit a semivariogram to the field. The optimized parameters of the model are $\nu = 2$ and $\ell = 0.019$, which corresponds to a practical range of 0.102. Thus, the values of the field are nearly independent a tenth of the way across the region. The sill and nugget are estimated to be $\sigma^2 = 1.003$ and $a_0 = 0.206$, respectively. A plot of the resulting fitted Matérn semivariogram model is given on the right side of Figure 3.

The values of ν and ℓ from $\boldsymbol{\theta} = (a_0, \sigma^2, \nu, \ell)$ obtained by fitting the Matérn semivariogram model to a spatial field, as described in the previous paragraph, can be used to define the Whittle-Matérn prior (17). The sill, σ^2 , and the nugget, a_0 , are not especially useful outside of fitting the semivariogram model because they do not correspond to any parameter in (17). They are helpful only in determining the best estimates for ν and ℓ . Any contribution these parameters may have made to the prior distribution will be accounted for in the regularization parameter, α . Therefore, after fitting the semivariogram models, σ^2 and a_0 are discarded.

With estimates for ν and ℓ in hand, the MAP estimator, \mathbf{x}_α , can then be computed as in Section 2.4, from which we can recompute $\boldsymbol{\theta}$ by fitting the Matérn semivariogram model to the empirical semivariogram values of \mathbf{x}_α . Repeating this process iteratively yields the following algorithm.

Algorithm: *The Semivariogram Method for MAP Estimation with Whittle-Matérn Prior:*

0. Estimate $\boldsymbol{\theta} = (a_0, \sigma^2, \nu, \ell)$ by fitting a Matérn semivariogram model to \mathbf{b} .
1. Define the prior (17) using ν and ℓ , compute α using (19), and compute \mathbf{x}_α using (18).

2. Update $\boldsymbol{\theta} = (a_0, \sigma^2, \nu, \ell)$ by fitting a Matérn semivariogram model to \mathbf{x}_α .
3. Return to step 1 and repeat until ν and ℓ stabilize.

Since ν is being optimized discretely to ensure that $\beta = \nu + d/2$ is an integer, convergence will be met when $\nu_j - \nu_{j-1} = 0$ where ν_j is the ν value fit in the j th iteration. Then ℓ is said to have converged when $|\ell_j - \ell_{j-1}|/\ell_{j-1} < \varepsilon$ with ε determined by the user. In this paper, we will consider ℓ to have converged when the relative difference is less than 0.01, which usually takes fewer than three iterations to achieve.

The semivariogram method is essentially a parametric empirical Bayes method [37] for point estimation. We have a distributional assumption on \mathbf{x} , but no prior distributions are assumed for ν or ℓ . The parameters are instead estimated by iteratively fitting semivariograms to the data.

3.1. Numerical Experiments

We now implement the semivariogram method on a two-dimensional deblurring and inpainting example. Recall that the connection between the Matérn covariance and the Whittle-Matérn prior depends on a stationarity assumption, which the following example may not exhibit. For simplicity, we will still assume stationarity and acknowledge that future work should be done in the case when no stationarity is present.

3.1.1. Results In this example, we assume periodic boundary conditions on the extended domain, but due to the restriction from the extended domain $\bar{\Omega}$ to Ω , circulant structure is lost in the forward model matrix, and hence, linear system solves must be done using an iterative method. As in [10, Section 3.1.3], we use preconditioned conjugate gradient (PCG) iteration, both for computing α and for computing \mathbf{x}_α . We attempt to deblur and demask a 128×128 image of Main Hall on the University of



Figure 4. Full 256×256 image of Main Hall at the University of Montana with 128×128 subimage.

Montana (UM) campus. To do this, we begin with a 256×256 image, given in Figure 4, and then restrict to the center 128×128 image. This smaller image in the middle will be thought of as being on a domain $\Omega = [0, 1] \times [0, 1]$ and the larger, full image will then be defined on $\bar{\Omega} = [-0.5, 1.5] \times [-0.5, 1.5]$.

To obtain \mathbf{b} , we first perform a slight blurring operation on the full 256×256 true image plotted in Figure 4. Since this is a color image, the deblurring process is done individually for the red, green, and blue intensity arrays. We then restrict to the central 128×128 pixels (with boundaries denoted in Figure 4) and randomly remove 40% of the pixels to obtain the masked, and moderately blurry image on the left in Figure 5.

We seek an estimate of \mathbf{x} in the same central subregion. Omnidirectional semivariograms with 25 approximately equally spaced grid points in $0 < r < \sqrt{2}/10$ are used. We chose $\sqrt{2}/10$ as a cutoff because it balances the need to capture the covariance structure at short distances, which are well-known to be the most important [34], with those at longer distances. When fitting semivariograms to the masked image, the removed entries will not be considered or else the correlation would be strongly influenced by those entries.

The semivariogram method is used to obtain $\nu = 1$ for each color band, $\ell = 0.0364, 0.0313$ and 0.0543 for the red, green, and blue intensities, respectively, and $\alpha = 0.0023, 0.0018$ and 5.47×10^{-5} . Convergence was met in two iterations for each color intensity. We also computed the Tikhonov solution, as defined in [10, Section 3.1.3], for which the prior covariance is equal to a scalar multiple of the identity matrix. The Tikhonov α values for all three color bands were around 0.0004. Note that for both of these reconstructions, the regularization parameter, α , was optimized using the highest correlation between the solution and the true image rather than chosen by GCV to ensure that any differences in the solutions is due to the method and not a poorly-chosen regularization parameter.

The two solutions are plotted in Figure 5. It is clear that the solution that used the Whittle-Matérn prior is the superior reconstruction. The correlation between \mathbf{x}_α and \mathbf{x} , the true image, is 0.950. While the Tikhonov solution is able to remove the blur, it performs inpainting poorly since each pixel value is assumed independent of one another due to the identity covariance matrix.

3.2. Discussion

Compared to the fully Bayesian method, the semivariogram procedure has some key advantages. This technique produces competitive solutions and clearer interpretations of the parameters ν and ℓ , and it can inform how far to extend the domain to maintain a connection with the Matérn covariance. Additionally, the computation time is only a fraction of what is needed to compute an adequate number of MCMC samples. In our implementation of the example above, the semivariogram method was more than 20 times faster than the fully Bayesian MCMC method. Finally, it is not trivial to sample from a complex model such as this one without significant autocorrelation, whereas

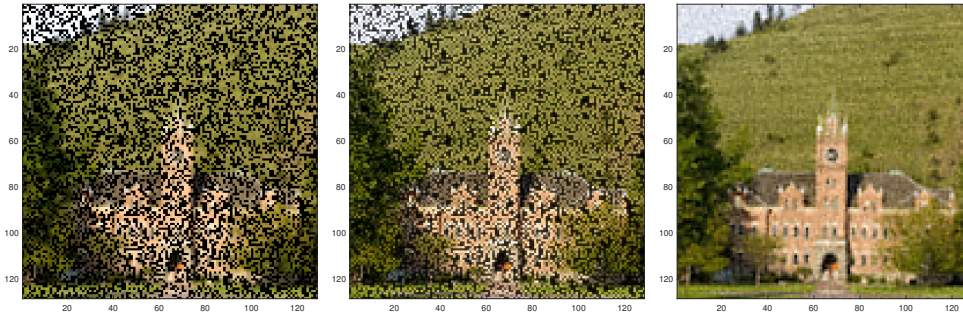


Figure 5. Two-dimensional image deblurring test case. On the left is a plot of the blurred, masked, and noisy data; in the middle is a plot of the Tikhonov solution; and on the right is a plot of the solution obtained using the Whittle-Matérn prior with $\nu = 1$ and $\ell = 0.0364, 0.0313$ and 0.0543 for red, green and blue intensities, respectively.

sampling is not needed for the semivariogram method.

The primary disadvantage is that we lose uncertainty quantification. We also have to calculate α , the regularization parameter, using other techniques like GCV. One other shortcoming to the semivariogram method, as described in this section, is the fact that it requires the field or image to be isotropic. In the next section, we extend these results to anisotropic fields.

4. Geometric Anisotropy

The solution to (6) is an isotropic Gaussian field, which means the correlation length is the same in every direction. This isotropy assumption is often not satisfied and so it will be useful to have an alternate SPDE formulation for the case when correlation lengths differ with direction. This is known as geometric anisotropy [34]. The groundwork for constructing priors that can model anisotropy has been laid in works such as [13, 7, 38].

4.1. Anisotropic SPDE

We will derive an anisotropic SPDE that can be used in similar way that (6) was used in the prior modeling in the isotropic case. We will only consider the two-dimensional case, but results can be extended to $d > 1$ dimensions. In two dimensions, for a Gaussian field with correlation length ℓ_1 in the direction of the angle θ , where $-\pi/2 < \theta \leq \pi/2$ is measured counter-clockwise from the x -axis, and correlation length ℓ_2 in the direction perpendicular to θ , we can make the following change of variables from isotropic to anisotropic coordinates:

$$\mathbf{w} = \begin{bmatrix} \cos \theta & -\ell_2/\ell_1 \sin \theta \\ \sin \theta & \ell_2/\ell_1 \cos \theta \end{bmatrix} \begin{bmatrix} u_1 \\ u_2 \end{bmatrix} \quad (23)$$

and thus

$$\begin{aligned} w_1(u_1, u_2) &= \cos \theta u_1 - \ell_2/\ell_1 \sin \theta u_2 \\ w_2(u_1, u_2) &= \sin \theta u_1 + \ell_2/\ell_1 \cos \theta u_2. \end{aligned}$$

We will apply the change of variables (23) to both sides of (6) to obtain the analogous anisotropic SPDE. The Laplacian on the left-hand side can be altered using the chain rule:

$$\begin{aligned}\frac{\partial}{\partial u_1} &= \frac{\partial}{\partial w_1} \frac{\partial w_1}{\partial u_1} + \frac{\partial}{\partial w_2} \frac{\partial w_2}{\partial u_1} \quad \text{and} \\ \frac{\partial}{\partial u_2} &= \frac{\partial}{\partial w_1} \frac{\partial w_1}{\partial u_2} + \frac{\partial}{\partial w_2} \frac{\partial w_2}{\partial u_2},\end{aligned}$$

which means

$$\begin{aligned}\frac{\partial^2}{\partial u_1^2} &= \left(\frac{\partial^2}{\partial w_1^2} \frac{\partial w_1}{\partial u_1} + \frac{\partial^2}{\partial w_1 \partial w_2} \frac{\partial w_2}{\partial u_1} \right) \frac{\partial w_1}{\partial u_1} + \left(\frac{\partial^2}{\partial w_1 \partial w_2} \frac{\partial w_1}{\partial u_1} + \frac{\partial^2}{\partial w_2^2} \frac{\partial w_2}{\partial u_1} \right) \frac{\partial w_2}{\partial u_1} \\ &= \cos^2 \theta \frac{\partial^2}{\partial w_1^2} + 2 \sin \theta \cos \theta \frac{\partial^2}{\partial w_1 \partial w_2} + \sin^2 \theta \frac{\partial^2}{\partial w_2^2}\end{aligned}$$

and

$$\begin{aligned}\frac{\partial^2}{\partial u_2^2} &= \left(\frac{\partial^2}{\partial w_1^2} \frac{\partial w_1}{\partial u_2} + \frac{\partial^2}{\partial w_2 \partial w_1} \frac{\partial w_2}{\partial u_2} \right) \frac{\partial w_1}{\partial u_2} + \left(\frac{\partial^2}{\partial w_1 \partial w_2} \frac{\partial w_1}{\partial u_2} + \frac{\partial^2}{\partial w_2^2} \frac{\partial w_2}{\partial u_2} \right) \frac{\partial w_2}{\partial u_2} \\ &= (\ell_2/\ell_1)^2 \sin^2 \theta \frac{\partial^2}{\partial w_1^2} - 2(\ell_2/\ell_1)^2 \sin \theta \cos \theta \frac{\partial^2}{\partial w_1 \partial w_2} + (\ell_2/\ell_1)^2 \cos^2 \theta \frac{\partial^2}{\partial w_2^2}.\end{aligned}$$

The right hand side of (6) is updated by changing the coordinates of the white noise. The inverse transformation of (23) is

$$\mathbf{u} = \begin{bmatrix} \cos \theta & \sin \theta \\ -\tau \sin \theta & \tau \cos \theta \end{bmatrix} \begin{bmatrix} w_1 \\ w_2 \end{bmatrix} := f(\mathbf{w}), \quad (24)$$

where $\tau = \ell_1/\ell_2$. Now, we define the transformed white noise basis functions as

$$\tilde{\phi}_j(\mathbf{w}) = \psi_j(f(\mathbf{w})) |\det(J_f(\mathbf{w}))|^{1/2} = \psi_j(f(\mathbf{w})) (\ell_1/\ell_2)^{1/2},$$

where $\det(J_f(\mathbf{w}))$ denotes the determinant of the Jacobian of the transformation $f(\mathbf{w})$, which is $(\ell_1/\ell_2)^{1/2}$ in our case. This will preserve the orthonormal properties of the basis functions. Then, appealing to (7),

$$\begin{aligned}\mathcal{W}(\mathbf{w}) &= \sum_{j=1}^{\infty} \xi_j \tilde{\phi}_j(\mathbf{w}), \quad \xi_j \stackrel{iid}{\sim} \mathcal{N}(0, \eta^2) \\ &= \sum_{j=1}^{\infty} \xi_j \phi_j(\mathbf{u}) (\ell_1/\ell_2)^{1/2} = (\ell_1/\ell_2)^{1/2} \mathcal{W}(\mathbf{u}),\end{aligned}$$

which means $\mathcal{W}(\mathbf{u}) = (\ell_2/\ell_1)^{1/2} \mathcal{W}(\mathbf{w})$.

So, taking $\ell = \ell_1$ and making the appropriate substitutions, (6) is converted to the anisotropic SPDE:

$$\left(1 - \left[(a_\theta^2 + b_\theta^2) \frac{\partial^2}{\partial w_1^2} + (c_\theta^2 + d_\theta^2) \frac{\partial^2}{\partial w_2^2} - 2(a_\theta c_\theta - b_\theta d_\theta) \frac{\partial^2}{\partial w_1 \partial w_2} \right] \right)^{\beta/2} x(\mathbf{w}) = (\ell_2/\ell_1)^{1/2} \mathcal{W}(\mathbf{w})$$

where $a_\theta = \ell_2 \sin \theta$, $b_\theta = \ell_1 \cos \theta$, $c_\theta = \ell_2 \cos \theta$, and $d_\theta = \ell_1 \sin \theta$. For

$$\mathbf{R} = \begin{bmatrix} \ell_1 \cos \theta & \ell_1 \sin \theta \\ -\ell_2 \sin \theta & \ell_2 \cos \theta \end{bmatrix},$$

the above SPDE can be written

$$(1 - \nabla \cdot \mathbf{R}^T \mathbf{R} \nabla)^{\beta/2} x(\mathbf{w}) = (\ell_2/\ell_1)^{1/2} \mathcal{W}(\mathbf{w}). \quad (25)$$

Notice that if $\ell_1 = \ell_2$, this SPDE is equivalent to (6) with $\ell = \ell_1$.

4.2. The Gaussian Field Solution of the SPDE (25)

Like in the isotropic case, we are interested in the the properties of the solution of (25), especially its covariance function. First, we define the anisotropic Matérn covariance function [39] as

$$C(r_w) = \sigma^2 \frac{(r_w/\zeta)^\nu K_\nu(r_w/\zeta)}{2^{\nu-1} \Gamma(\nu)}, \quad \text{with } \zeta = \frac{\ell_1}{\sqrt{\cos^2(\psi - \theta) + (\ell_1/\ell_2)^2 \sin^2(\psi - \theta)}}, \quad (26)$$

where $r_w = \|\mathbf{w}_i - \mathbf{w}_j\|$ is the distance between the anisotropic coordinates, ζ is the new range parameter in the direction of ψ , ℓ_1 is the correlation length in the direction of θ and ℓ_2 is the correlation length in the direction perpendicular to θ . Notice that the smoothness parameter, ν , is unaffected.

The remainder of this subsection contains results used to prove the following theorem.

Theorem 2 *The solution $x(\mathbf{w})$ of (25) is a Gaussian field with mean zero and anisotropic Matérn covariance function defined by (26).*

Proof. First, we derive the Green's function for (25), which is the solution of

$$(1 - \nabla \cdot \mathbf{R}^T \mathbf{R} \nabla)^{\beta/2} g(\mathbf{w}, \mathbf{v}) = \delta(\mathbf{v} - \mathbf{w}). \quad (27)$$

Using (8), the solution to (25) is given by

$$x(\mathbf{w}) = (\ell_2/\ell_1)^{1/2} \int_{\mathbb{R}^2} g(\mathbf{w}, \mathbf{v}) \mathcal{W}(\mathbf{v}) d\mathbf{v}, \quad (28)$$

which makes $x(\mathbf{w})$ a Gaussian field since it is a linear transformation of Gaussian white noise. Be aware that we are still assuming stationarity in our field. To derive the Green's function g in (28), we first define $g(\mathbf{w}) := g(\mathbf{w}, \mathbf{0})$. Then (27) implies

$$(1 - \nabla \cdot \mathbf{R}^T \mathbf{R} \nabla)^{\beta/2} g(\mathbf{w}) = \delta(\mathbf{w}). \quad (29)$$

We would like to change from the anisotropic coordinates \mathbf{w} to anisotropic coordinates \mathbf{u} in (29) so we can use the results from Section 2.2. We again use (24) for the coordinate change and, in a similar fashion as was done earlier, we apply the chain rule to replace $\partial^2/\partial w_1^2$, $\partial^2/\partial w_2^2$, and $\partial^2/(\partial w_1 \partial w_2)$ in $(1 - \nabla \cdot \mathbf{R}^T \mathbf{R} \nabla)^{\beta/2}$ with partial derivatives in terms of \mathbf{u} . When making this change, the coefficients of $\partial^2/\partial u_1^2$, $\partial^2/\partial u_2^2$, and $\partial^2/(\partial u_1 \partial u_2)$ are ℓ_1^2 , ℓ_1^2 , and 0, respectively and so we have $(1 - \nabla \cdot \mathbf{R}^T \mathbf{R} \nabla)g(\mathbf{w}) = (1 - \ell_1^2 \Delta)g(\mathbf{u})$. Additionally, we can change variables in the Delta function on the right side of (29) by multiplying by the determinant of the Jacobian of (24): ℓ_1/ℓ_2 . Thus, the change of variables transforms (29) into the equation

$$(1 - \ell_1^2 \Delta)^{\beta/2} g(\mathbf{u}) = (\ell_1/\ell_2) \delta(\mathbf{u}), \quad (30)$$

which is equivalent to (12) up to a constant. Hence, we can apply the results of Section 2.2. Namely, after changing variables, the solution of (25) is a Gaussian field with mean zero and the isotropic Matérn covariance function defined by (5). Notice that the constant that multiplies the Delta function on the right-hand side of (30) and the constant that multiplies the integral in (28) will cancel when going through the process of deriving the covariance function since the constant in (28) gets squared.

We must now make one final change of variables back to \mathbf{w} from \mathbf{u} so our covariance function will be in terms of the anisotropic coordinates rather than the isotropic ones. Since the input to the Matérn correlation function must be a distance between isotropic spatial locations, we need to represent an isotropic distance, r_u , in terms of the anisotropic coordinates. Consider $\mathbf{r} := \mathbf{w}_i - \mathbf{w}_j$. Then, defining $r_w := \|\mathbf{r}\| = \|\mathbf{w}_i - \mathbf{w}_j\|$,

$$\begin{aligned} r_u := \|\mathbf{u}_i - \mathbf{u}_j\| &= \left\| \begin{bmatrix} \cos \theta & \sin \theta \\ -\tau \sin \theta & \tau \cos \theta \end{bmatrix} (\mathbf{w}_i - \mathbf{w}_j) \right\| = \left\| \begin{bmatrix} \cos \theta & \sin \theta \\ -\tau \sin \theta & \tau \cos \theta \end{bmatrix} \mathbf{r} \right\| \\ &= \left\| \begin{bmatrix} \cos \theta & \sin \theta \\ -\tau \sin \theta & \tau \cos \theta \end{bmatrix} \begin{bmatrix} r_1 \\ r_2 \end{bmatrix} \right\| = \left\| \begin{bmatrix} r_1 \cos \theta + r_2 \sin \theta \\ -r_1 \tau \sin \theta + r_2 \tau \cos \theta \end{bmatrix} \right\|. \end{aligned}$$

Now we convert to polar coordinates with $r_1 = r_w \cos \psi$ and $r_2 = r_w \sin \psi$. Then

$$\begin{aligned} r_u &= \left\| \begin{bmatrix} r_w \cos \psi \cos \theta + r_w \sin \psi \sin \theta \\ -r_w \tau \cos \psi \sin \theta + r_w \tau \sin \psi \cos \theta \end{bmatrix} \right\| = \left\| \begin{bmatrix} r_w \cos(\psi - \theta) \\ r_w \tau \sin(\psi - \theta) \end{bmatrix} \right\| \\ &= r_w [\cos^2(\psi - \theta) + \tau^2 \sin^2(\psi - \theta)]^{1/2}. \end{aligned}$$

Therefore, we need to adjust the distance between the vectors \mathbf{w}_i and \mathbf{w}_j by $[\cos^2(\psi - \theta) + \tau^2 \sin^2(\psi - \theta)]^{1/2}$ in order to get the distances to plug into the isotropic Matérn correlation function. Thus, the isotropic Matérn covariance function has been generalized to the anisotropic case using the same change of variables as in (23). Adjusting the anisotropic distances is equivalent to defining the anisotropic Matérn covariance function as we have in (26). \square

4.3. Anisotropic Prior Modeling

To obtain a sparse representation of the precision matrix for the anisotropic Matérn covariance, we can discretize (25) using the standard finite-difference approximations with appropriate boundary conditions. Taking a step size of $h = 1/n$ on a uniform mesh, so that $N = n^2$ in two dimensions, yields

$$\begin{aligned} &\left[\mathbf{I} + \frac{1}{h^2} (a_\theta^2 + b_\theta^2) (\mathbf{L} \otimes \mathbf{I}) + \frac{1}{h^2} (c_\theta^2 + d_\theta^2) (\mathbf{I} \otimes \mathbf{L}) \right. \\ &\quad \left. - \frac{2}{4h^2} (a_\theta c_\theta - b_\theta d_\theta) (\mathbf{K} \otimes \mathbf{K}) \right]^{\beta/2} \mathbf{x} = \delta^{-1/2} \boldsymbol{\xi}, \quad \boldsymbol{\xi} \sim \mathcal{N}(\mathbf{0}, \mathbf{I}_N). \end{aligned}$$

where \otimes denotes Kronecker product [10]. Note that the constant multiplying the white noise term gets absorbed into the δ parameter.

In the zero boundary condition case,

$$\mathbf{L} = \begin{bmatrix} 2 & -1 & 0 & \dots & 0 \\ -1 & 2 & -1 & \dots & 0 \\ 0 & -1 & 2 & \ddots & \vdots \\ \vdots & \ddots & \ddots & \ddots & -1 \\ 0 & 0 & \dots & -1 & 2 \end{bmatrix}_{n \times n} \quad \text{and} \quad \mathbf{K} = \begin{bmatrix} 0 & 1 & 0 & \dots & 0 \\ -1 & 0 & 1 & \dots & 0 \\ 0 & -1 & 0 & \ddots & \vdots \\ \vdots & \ddots & \ddots & \ddots & 1 \\ 0 & 0 & \dots & -1 & 0 \end{bmatrix}_{n \times n},$$

and when using periodic boundary conditions, we let $\mathbf{L}(1, n) = \mathbf{L}(n, 1) = \mathbf{K}(1, n) = -1$ and $\mathbf{K}(n, 1) = 1$. Then

$$\mathbf{x} \sim \mathcal{N}(\mathbf{0}, \delta^{-1} \mathbf{P}^{-1}) \quad (31)$$

where

$$\mathbf{P} = \left[\mathbf{I} + \frac{1}{h^2} (a_\theta^2 + b_\theta^2) (\mathbf{L} \otimes \mathbf{I}) + \frac{1}{h^2} (c_\theta^2 + d_\theta^2) (\mathbf{I} \otimes \mathbf{L}) - \frac{2}{4h^2} (a_\theta c_\theta - b_\theta d_\theta) (\mathbf{K} \otimes \mathbf{K}) \right]^\beta. \quad (32)$$

In order to retain sparsity in \mathbf{P} , we will again require that $\beta = \nu + d/2$ be an integer. Additionally, like in the isotropic case, an extension of the computational domain is required to maintain a connection between (32) and (26).

Now that we have a prior covariance matrix that maintains a connection to the anisotropic Matérn covariance, we return to the MAP estimator, which can be computed by solving

$$\begin{aligned} \mathbf{x}_\alpha &= \arg \min_{\mathbf{x}} \left\{ \frac{1}{2} \|\mathbf{A}\mathbf{x} - \mathbf{b}\|^2 + \frac{\alpha}{2} \mathbf{x}^T \mathbf{P} \mathbf{x} \right\} \\ &= (\mathbf{A}^T \mathbf{A} + \alpha \mathbf{P})^{-1} \mathbf{A}^T \mathbf{b}, \end{aligned} \quad (33)$$

where $\alpha = \delta/\lambda$ and \mathbf{P} is as in (32).

4.4. Directional Semivariograms

When fitting semivariograms to a spatial field, intrinsic stationarity and isotropy is assumed. In our case, we are still assuming intrinsic stationarity, but our field is anisotropic. Thus, a change must be made to our field before fitting a semivariogram to obtain an estimate for ℓ_1 and ℓ_2 . We again use (24), the inverse of the change used in (23). Using the same argument that was used when transforming the Green's function PDE from anisotropic coordinates in (29) to isotropic coordinates in (30), it is not difficult to show that (25) is transformed to

$$(1 - \ell_1^2 \Delta)^{(\nu+d/2)/2} x(\mathbf{u}) = \mathcal{W}(\mathbf{u}),$$

which is equivalent to (6) with $\ell = \ell_1$.

We can apply this same change of variables (24) to any two-dimensional spatial field that exhibits geometric anisotropy to achieve isotropy. For example, if we begin with a spatial field that exhibits its larger correlation length in the 45° direction with $\tau = \ell_1/\ell_2 = 3$, the change of variables will rotate the field so the direction of maximum correlation length is in the 0° direction and will then stretch the field along the new

y -axis to remove the geometric anisotropy and create a new, isotropic field. This is shown in the middle in Figure 6. Once the spatial field has been adjusted in this way, a semivariogram can be fit to the transformed field as in the usual, isotropic case.

In order to adjust the spatial field to satisfy the isotropy assumptions in the way described above, we must ascertain θ , the direction of maximum correlation length measured from the x -axis, and τ , the ratio of the correlation length in the direction of θ to the correlation length in the direction orthogonal to θ . Both of these parameters can be estimated using directional empirical semivariograms. Directional semivariograms are fit in a similar way as omnidirectional semivariograms in (20), but instead of taking all points separated by a distance r , we restrict the pairs of points to a certain angle, ψ . If we think of \mathbf{w}_i and \mathbf{w}_j as vectors, then ψ is equivalent to the angle between $\mathbf{w}_i - \mathbf{w}_j$ and the x -axis. For example, if $\psi = 0$, we restrict to all pairs of locations w_i and w_j on the same horizontal line, i.e., with the same y -coordinate. Formally, the empirical directional semivariogram can be defined as

$$\hat{\gamma}_\psi(r) = \frac{1}{2n(r, \psi)} \sum_{(i,j) \parallel \|\mathbf{w}_i - \mathbf{w}_j\| = r, \phi_{ij} = \psi} [x(\mathbf{w}_i) - x(\mathbf{w}_j)]^2, \quad (34)$$

where ϕ_{ij} denotes the angle between $\mathbf{w}_i - \mathbf{w}_j$ and the x -axis, and $n(r, \psi)$ is the number of points that are separated by a distance r with angle of separation equal to ψ . It is common to calculate a directional semivariogram for $-90^\circ < \psi \leq 90^\circ$ in steps of either 15° or 30° . We take a step size of 15° here, which will result in 12 directional semivariograms.

Once the directional semivariograms have been calculated for each of the 12 different ψ angles, we fit a common scatterplot smoother, the loess curve [40], to the semivariogram values in each direction to achieve continuous curves. Then, to determine the ratio of correlation lengths, we can select a constant γ_{crit} value between the nugget and sill and observe the distance required for the loess curve to surpass the height of γ_{crit} . The direction of maximum correlation, θ , will require a larger distance to reach γ_{crit} than other directions since the variance of the differences between values in that direction is expected to be smaller. The anisotropy ratio, τ , can then be computed as the ratio between the distance in the direction of θ and the distance in the direction perpendicular to θ .

This process is illustrated in Figure 6. The directional semivariograms are shown for the original, anisotropic field on the left. We can see that the correlation length is largest in the 45° direction since the distance of 0.1684 that it takes for the curve to pass $\gamma_{\text{crit}} = 0.9$ is the largest of any direction. The range distance in the -45° direction is 0.0561 and so the ratio of those ranges is $\tau = 0.1684/0.0561 = 3$.

We can then rotate the field clockwise by 45° and stretch it in the direction of the new y -axis by a factor of $\tau = 3$ to achieve an isotropic field, as is done in the middle of Figure 6. The directional semivariograms for the new field are shown on the right in Figure 6. It now takes a distance of 0.1684 for the variogram values to pass γ_{crit} for each ψ angle, which means the ratio has been reduced to one, as it should be for an isotropic

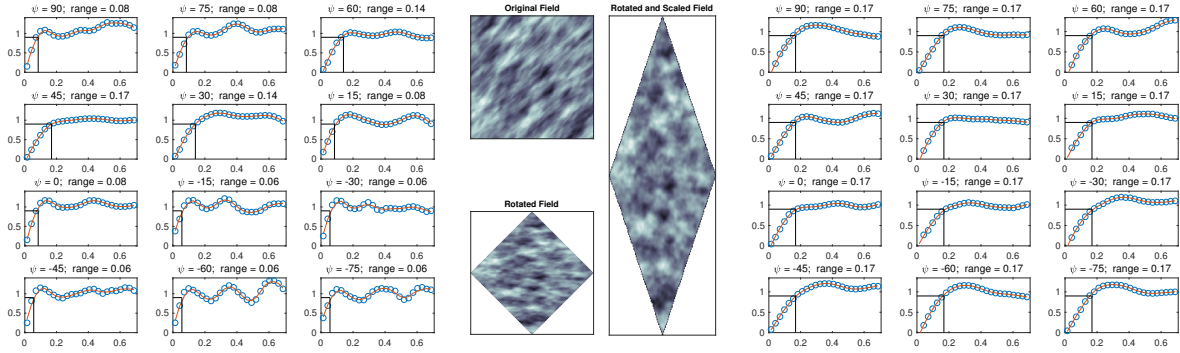


Figure 6. Directional semivariograms. The directional semivariograms for the original, anisotropic field are shown on the left. For each of the 12 images, semivariogram value is plotted against lag distances. The direction of maximum correlation is determined to be 45° with a ratio of 3 since the distance required to pass $\gamma_{\text{crit}} = 0.9$ was largest in that direction and that distance is 3 times greater than the distance needed in the -45° direction. The directional semivariograms for the rotated and scaled field are shown on the right with a ratio of 1.

field. It is not always the case that we can reduce the ratio of these range values down to one, but we can reduce it enough for the field to be considered approximately isotropic.

Once we have obtained θ and τ and have changed the coordinates of the field, we can fit an isotropic omnidirectional semivariogram to estimate ν and ℓ_1 . Then we let $\ell_2 = \ell_1/\tau$. All parameters for use in (31) will have been estimated and we can update these estimates iteratively.

Algorithm: *The Semivariogram Method for MAP Estimation with Anisotropic Whittle-Matérn Prior:*

0. Set $\mathbf{x}_\alpha = \mathbf{b}$.
1. Estimate θ and τ by computing directional semivariograms for \mathbf{x}_α .
2. Transform the anisotropic spatial field coordinates, \mathbf{w} , to isotropic spatial field coordinates, \mathbf{u} , using (24).
3. Estimate $\boldsymbol{\theta} = (a_0, \sigma^2, \nu, \ell_1)$ by fitting an isotropic Matérn semivariogram model to the transformed field. Then compute $\ell_2 = \ell_1/\tau$.
4. Define the prior precision matrix, \mathbf{P} , by (32) using ν , ℓ_1 , ℓ_2 , and θ , compute α using (19), and compute \mathbf{x}_α using (33).
5. Return to step 1 and repeat until θ , τ , ν , ℓ_1 , and ℓ_2 stabilize.

The convergence criteria for these parameters are as follows: $\theta_j - \theta_{j-1} = 0$, $\nu_j - \nu_{j-1} = 0$, $|\ell_1^j - \ell_1^{j-1}|/\ell_1^{j-1} < 0.01$, and $|\ell_2^j - \ell_2^{j-1}|/\ell_2^{j-1} < 0.01$ where $\theta_j, \nu_j, \ell_1^j$ and ℓ_2^j denotes the j th iteration of the respective parameter.

4.5. Numerical Experiments

We will illustrate the semivariogram method in the anisotropic case with a two-dimensional inpainting example. The original image, given on the left in Figure 7,

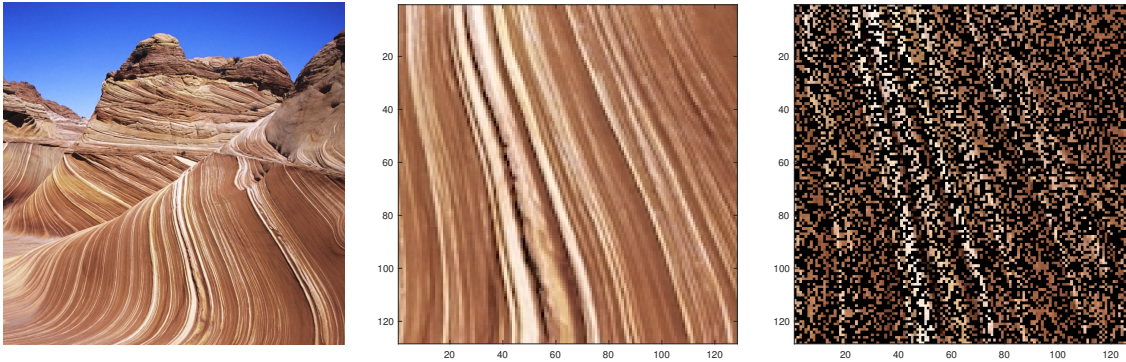


Figure 7. Inpainting example. The original image showing the rock layers of the Wave in northern Arizona is given on the left. The true image used in the inpainting example is given in the middle. The masked image is given on the right.

shows a rock formation in Northern Arizona known as the Wave [41] where the layers of sandstone strata are clearly visible. We selected a subsection in the lower-middle of the image, shown in the middle of Figure 7, to illustrate our method. This will be the true image. We then added some noise and masked 60% of the image. This is shown on the right in Figure 7.

Like we saw in Section 3.1.1, the prior will play a large role in the inpainting process since much of the image is missing. We will directly compare the solution using the anisotropic Whittle-Matérn prior to the solution using the isotropic Whittle-Matérn prior, both of which will have parameters determined using semivariograms. Like before, the regularization parameter, α , will be optimized using the highest correlation between the solution and the true image.

After calculating the directional semivariograms for the image, the direction of maximum correlation was determined to be -75° for each color intensity. For the blue color-band, the correlation length in that direction was $\ell_1 = 0.1517$ and the correlation in the 15° direction was $\ell_2 = 0.0101$, which gives a ratio of $\tau = 15$. ν was determined to be 1 and all of these parameters converged in at most four iterations for each color. When fitting an omnidirectional semivariogram to the masked image for the isotropic case, $\nu = 2$ and $\ell = 0.0142$.

The reconstructions are given in Figure 8. With the isotropic solution, the masking is removed, but since the prior assigns a very small correlation between each pixel, the reconstruction is noticeably spotty. The anisotropic solution, however, does a good job of removing the masking completely. The reconstruction is a bit smoother than the true image, but the original sandstone layers can be seen nicely.

Some statistics of the reconstructions are given in Table 1. Although the isotropic solution is still competitive, the anisotropic prior gives the reconstruction that most closely aligns with the true image. The isotropic solution has a mean absolute error (MAE) more than 57% larger and a mean squared error (MSE) more than 180% higher than those respective measures in the anisotropic case. The anisotropic reconstruction does fall short with the minimum value, however, which is farther from the truth than

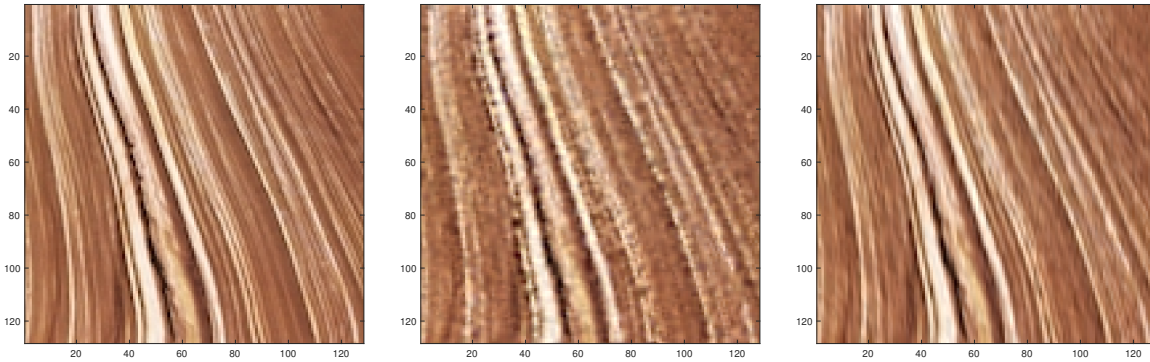


Figure 8. Inpainting solutions. The true image (left) is given along with the the isotropic solution (middle) and the anisotropic solution (right).

Table 1. Statistics for inpainting MAP estimates.

	True Image	Isotropic Covariance	Anisotropic Covariance
\bar{x}	0.530	0.530	0.530
s	0.207	0.202	0.206
Min	0.000	-0.053	-0.065
Q_1	0.357	0.364	0.360
Median	0.522	0.520	0.520
Q_3	0.678	0.676	0.678
Max	1.000	1.112	1.093
$\rho_{\mathbf{x}_\alpha, \mathbf{x}_{\text{true}}}$		0.944	0.981
Residual MAE		0.045	0.029
Residual MSE		0.005	0.002

the solution given by the isotropic prior.

4.6. Discussion

Although the reconstruction with the anisotropic prior covariance matrix is better here, there are still some improvements that can be made. This example had a constant angle of maximum correlation length throughout the image and the ratio between maximum and minimum correlation was rather high, that is, greater than five. If either of these features fail to hold, the anisotropic prior often produces a reconstruction that performs slightly worse or offers no benefit over using an isotropic prior. We focus on the case when the angle of maximum anisotropy is not constant in the next section.

5. Regional Anisotropy

We have a way to define priors for isotropic and anisotropic spatial fields as long as that covariance structure is consistent for the entire field. In the case where the correlation length and angle of maximum anisotropy change throughout the image, we will want to

model each of these regions with a different prior.

5.1. Regional Precision Matrix

Suppose we have k different regions in our image, each of which has a different covariance structure. We define \mathbf{D}_i , $i = 1, \dots, k$, as a masking matrix such that the only non-zero elements of $\mathbf{D}_i \mathbf{x}$ are those in region i . We will not allow for overlapping regions so that $\sum_{i=1}^k \mathbf{D}_i = \mathbf{I}$, the identity matrix. Now, to establish a prior for \mathbf{x} in this regional case, we take $\text{Cov}(\mathbf{x}) = \text{Cov}(\mathbf{D}_1 \mathbf{x} + \dots + \mathbf{D}_k \mathbf{x}) = \text{Cov}(\mathbf{D}_1 \mathbf{x}) + \dots + \text{Cov}(\mathbf{D}_k \mathbf{x})$, since each region is assumed independent due to not having any elements of \mathbf{x} in common. Define the best Whittle-Matérn covariance structure, as chosen by a semivariogram, for region i as \mathbf{C}_i with corresponding precision matrix $\mathbf{P}_i = \mathbf{C}_i^{-1}$. Then $\text{Cov}(\mathbf{D}_i \mathbf{x}) := \mathbf{D}_i \mathbf{C}_i \mathbf{D}_i$. Thus, the prior for \mathbf{x} in this regional case has pdf

$$p(\mathbf{x}|\delta) \propto \exp\left(-\frac{\delta}{2} \mathbf{x}^T (\mathbf{D}_1 \mathbf{C}_1 \mathbf{D}_1 + \dots + \mathbf{D}_k \mathbf{C}_k \mathbf{D}_k)^{-1} \mathbf{x}\right), \quad (35)$$

which means our precision matrix is given by $\mathbf{P} = (\mathbf{D}_1 \mathbf{C}_1 \mathbf{D}_1 + \dots + \mathbf{D}_k \mathbf{C}_k \mathbf{D}_k)^{-1}$. Note that (35) reduces to (3) with $\mathbf{P} = \mathbf{P}_1$ when $k = 1$. In general, the \mathbf{C}_i matrices and \mathbf{P} are dense, so actually constructing this precision matrix is infeasible for large problems. Additionally, FFTs cannot be used since $\mathbf{D}_1 \mathbf{C}_1 \mathbf{D}_1 + \dots + \mathbf{D}_k \mathbf{C}_k \mathbf{D}_k$ is not circulant even if each \mathbf{C}_i is. Thus, we seek an alternative expression such that the matrix-vector multiplication $\mathbf{P} \mathbf{x}$ is achievable.

Without loss of generality, let $k = 2$. Let

$$\mathbf{C}_1 = \begin{bmatrix} C_{1A} & C_{1B} \\ C_{1C} & C_{1D} \end{bmatrix} = \mathbf{P}_1^{-1} = \begin{bmatrix} P_{1A} & P_{1B} \\ P_{1C} & P_{1D} \end{bmatrix}^{-1}$$

and

$$\mathbf{C}_2 = \begin{bmatrix} C_{2A} & C_{2B} \\ C_{2C} & C_{2D} \end{bmatrix} = \mathbf{P}_2^{-1} = \begin{bmatrix} P_{2A} & P_{2B} \\ P_{2C} & P_{2D} \end{bmatrix}^{-1}.$$

Also assume that the regions are defined in a way that divides the region vertically (an assumption we will drop later) so that

$$\mathbf{C} = \text{Cov}(\mathbf{x}) = \text{Cov}(\mathbf{D}_1 \mathbf{x} + \mathbf{D}_2 \mathbf{x}) = \text{Cov}(\mathbf{D}_1 \mathbf{x}) + \text{Cov}(\mathbf{D}_2 \mathbf{x}) = \begin{bmatrix} C_{1A} & 0 \\ 0 & C_{2D} \end{bmatrix},$$

which means our precision matrix is

$$\mathbf{P} = \mathbf{C}^{-1} = \begin{bmatrix} C_{1A}^{-1} & 0 \\ 0 & C_{2D}^{-1} \end{bmatrix}.$$

Using the block matrix inversion identity, it can be shown that $C_{1A}^{-1} = P_{1A} - P_{1B} P_{1D}^{-1} P_{1C}$ and $C_{2D}^{-1} = P_{2D} - P_{2C} P_{2A}^{-1} P_{2B}$ and thus

$$\mathbf{P} = \mathbf{C}^{-1} = \begin{bmatrix} C_{1A}^{-1} & 0 \\ 0 & C_{2D}^{-1} \end{bmatrix} = \begin{bmatrix} P_{1A} - P_{1B} P_{1D}^{-1} P_{1C} & 0 \\ 0 & P_{2D} - P_{2C} P_{2A}^{-1} P_{2B} \end{bmatrix},$$

which can be equivalently written as

$$\mathbf{P} = \mathbf{D}_1 \mathbf{P}_1 \mathbf{D}_1 - \mathbf{D}_1 \mathbf{P}_1 (\mathbf{D}_2 \mathbf{P}_1 \mathbf{D}_2)^\dagger \mathbf{P}_1 \mathbf{D}_1 + \mathbf{D}_2 \mathbf{P}_2 \mathbf{D}_2 - \mathbf{D}_2 \mathbf{P}_2 (\mathbf{D}_1 \mathbf{P}_2 \mathbf{D}_1)^\dagger \mathbf{P}_2 \mathbf{D}_2.$$

In general, for $k > 2$,

$$\begin{aligned} \mathbf{P} &= \mathbf{C}^{-1} = (\mathbf{D}_1 \mathbf{P}_1 \mathbf{D}_1 + \mathbf{D}_2 \mathbf{P}_2 \mathbf{D}_2 + \dots + \mathbf{D}_k \mathbf{P}_k \mathbf{D}_k)^{-1} \\ &= \sum_{i=1}^k \left(\mathbf{D}_i \mathbf{P}_i \mathbf{D}_i - \mathbf{D}_i \mathbf{P}_i \left[(\mathbf{I}_N - \mathbf{D}_i) \mathbf{P}_i (\mathbf{I}_N - \mathbf{D}_i) \right]^\dagger \mathbf{P}_i \mathbf{D}_i \right), \end{aligned} \quad (36)$$

which, since each \mathbf{P}_i is sparse, involves only sparse matrices. It is straightforward to show (36) holds even in the case where the regions do not divide the region vertically by performing a reordering of the indices of \mathbf{x} .

Since we have an expression for \mathbf{P} , we can now discuss how to perform the multiplication $\mathbf{P}\mathbf{x}$. This will be needed to perform an iterative inverse method such as conjugate gradient to obtain the MAP estimator. Since each \mathbf{D}_i and \mathbf{P}_i is sparse, each matrix vector multiplication in (36) is efficient except the ones involving pseudoinverses. We can, however, take advantage of the lower-rank structure of $((\mathbf{I}_N - \mathbf{D}_i) \mathbf{P}_i (\mathbf{I}_N - \mathbf{D}_i))^\dagger$, which has rank $N - r_i$ where r_i the rank of \mathbf{D}_i . Let $\mathbf{P}_{i,\text{nz}}$ be the square matrix that consists of all rows and columns of $(\mathbf{I}_N - \mathbf{D}_i) \mathbf{P}_i (\mathbf{I}_N - \mathbf{D}_i)$ that have any nonzero elements. That is, keep row and column j of $(\mathbf{I}_N - \mathbf{D}_i) \mathbf{P}_i (\mathbf{I}_N - \mathbf{D}_i)$ if $[\mathbf{I}_N - \mathbf{D}_i]_{j,j} = 1$. Then let $\mathbf{R}_i = \text{chol}(\mathbf{P}_{i,\text{nz}})$ such that $\mathbf{P}_{i,\text{nz}} = \mathbf{R}_i^T \mathbf{R}_i$ where chol denotes the Cholesky factorization and \mathbf{R}_i is upper triangular. The Cholesky decomposition is known to be efficient for sparse, symmetric, positive definite matrices such as $\mathbf{P}_{i,\text{nz}}$ [42]. Then we can perform the multiplication of $\mathbf{D}_i \mathbf{P}_i \left((\mathbf{I}_N - \mathbf{D}_i) \mathbf{P}_i (\mathbf{I}_N - \mathbf{D}_i) \right)^\dagger \mathbf{P}_i \mathbf{D}_i \mathbf{x}$ in the following way:

1. Multiply $\mathbf{y}_i = \mathbf{P}_i (\mathbf{D}_i \mathbf{x})$.
2. Extract the $N - r_i$ elements of \mathbf{y}_i that correspond to the nonzero diagonal elements of $\mathbf{I}_N - \mathbf{D}_i$: $\mathbf{y}_i(\text{ind})$.
3. Define a variable \mathbf{z}_i as an $N \times 1$ vector of zeros.
4. Multiply by $\left((\mathbf{I}_N - \mathbf{D}_i) \mathbf{P}_i (\mathbf{I}_N - \mathbf{D}_i) \right)^\dagger$ by taking $\mathbf{z}_i(\text{ind}) = \mathbf{R}_i \setminus (\mathbf{R}_i^T \setminus \mathbf{y}_i(\text{ind}))$.
5. Complete the multiplication $\mathbf{D}_i (\mathbf{P}_i \mathbf{z}_i)$.
6. Repeat for $1 \leq i \leq k$, so $\mathbf{P}\mathbf{x} = \sum_{i=1}^k \mathbf{D}_i (\mathbf{P}_i \mathbf{z}_i)$.

Step 4 is the most costly since it requires both a forward and a backward substitution. This can be performed more efficiently for large regions since the rank of $(\mathbf{I}_N - \mathbf{D}_i) \mathbf{P}_i (\mathbf{I}_N - \mathbf{D}_i)$ is inversely related to the size of region i . Also, sparse reorderings, such as the symmetric approximate minimum degree permutation, can be used so \mathbf{R}_i has fewer nonzero entries. The multiplication of $\mathbf{P}\mathbf{x}$ must be performed for each iteration of CG, but each \mathbf{R}_i can be stored ahead of time so the Cholesky decompositions need only be performed once. We saw some improvements in the performance of the CG algorithm when a preconditioner was used. The total number of iterations was approximately 21% lower, which corresponded to about a 15% overall time saving.

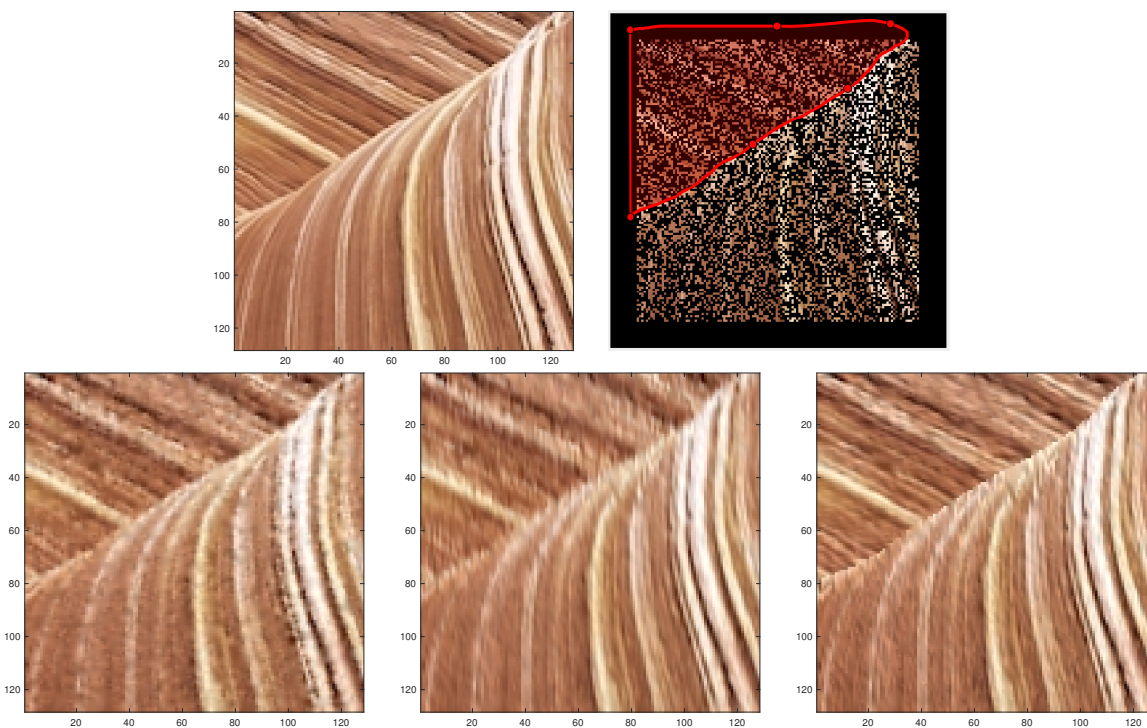


Figure 9. Inpainting solutions. The true image (top-left) is given along with the masked image (top-right), the isotropic solution (bottom-left) and the anisotropic solution (bottom-middle), and the regional solution (bottom-right).

5.2. Numerical Experiments

We now consider an example where the angle of maximum anisotropy changes throughout the image. We take the central portion of the Wave image from Figure 7 and again mask it so that 60% of the image is blank. Then we attempt to inpaint the image using an isotropic prior, an anisotropic prior, and a regional anisotropic prior. The results are shown in Figure 9. The top-right image shows the masked picture as well as how the regions were chosen. The first region is shown with the red overlay while the second region is the remainder of the image. Semivariograms were fit to both regions and the top region was given a prior with an angle of maximum anisotropy of -30° while $\theta = -75^\circ$ for the bottom region. In the anisotropic solution given in the bottom-middle of the figure, $\theta = -75^\circ$ throughout the image. Qualitatively, the regional solution in the bottom-right of the figure looks best.

Turning to Table 2, we can see the statistics comparing the different reconstructions. The isotropic and anisotropic solutions were similar in terms of the correlation and mean errors, but the regional solution is better in both of those categories and is similar in the others.

Table 2. Statistics for regional inpainting MAP estimates.

	True Image	Isotropic Covariance	Anisotropic Covariance	Regional Covariance
\bar{x}	0.567	0.565	0.566	0.566
s	0.207	0.200	0.202	0.207
Min	0.000	-0.014	-0.082	-0.032
Q_1	0.400	0.402	0.402	0.398
Median	0.565	0.564	0.564	0.562
Q_3	0.722	0.717	0.718	0.720
Max	1.000	1.085	1.077	1.160
$\rho_{\mathbf{x}_\alpha, \mathbf{x}_{\text{true}}}$		0.954	0.954	0.969
Residual MAE		0.042	0.041	0.035
Residual MSE		0.004	0.004	0.003

5.3. Discussion

The regional covariance solution performed better in this example, but it does have some shortcomings. Firstly, it is best used when the distinction between regions is high. This is because the transition between regions when using this prior is abrupt, rather than smooth. Smoothing the transition between regions is something we leave to future work. Additionally, since multiplying \mathbf{P} by \mathbf{x} requires inverting a matrix, this method can be slow when that matrix is large, which corresponds to a small region. Therefore, we suggest using small regions only when necessary. Alternatively, it is possible to solve a different inverse problem for each region independently and then combine the results. This will allow FFTs to be used since the precision matrix for each inverse problem will be in the form of 32.

6. Conclusion

In this paper, we introduced a method for selecting parameters for use in the prior distribution of \mathbf{x} based on semivariogram modeling. We think of the noisy data as a spatial field and fit semivariograms to the noisy data and then iteratively to the MAP estimates to obtain point estimates for the prior parameters. This method relies on the fact that the solution of the SPDE (6) is a Gaussian process with zero mean and Matérn covariance operator, which we have shown in detail. However, this connection requires an infinite domain, for us \mathbb{R}^2 . For a finite domain, which is typically required for computations, the connection is broken, i.e., the SPDE solution is a zero mean Gaussian process without a Matérn covariance operator. Fortunately, the connection can be restored by extending the finite computational domain. We showed how to systematically choose the extended domain using the Matérn parameters. The semivariogram method has the benefits of giving point estimates with a more intuitive interpretation while providing an objective way to choose an extension of the computational domain that is adequate for restoring the SPDE/Matérn connection.

We then applied the semivariogram method to an isotropic inpainting and deblurring example in two dimensions.

We generalized the isotropic results to the anisotropic case and showed the semivariogram method can be applied as well by using directional semivariograms and the anisotropic SPDE (25). An inpainting example comparing reconstructions using isotropic and anisotropic priors was presented. Finally, we discussed an even more general case when the image has regions with differing correlation lengths and angles of maximum correlation, which requires a sparse precision matrix that can be obtained via a discretized SPDE for each region. One more example was shown that yielded good solutions.

Acknowledgments

We would like to acknowledge the assistance of Dr. Jon Graham at the University of Montana with the semivariogram methodology.

References

- [1] Jari Kaipio and Erkki Somersalo. *Statistical and Computational Methods for Inverse Problems*. Springer, 2005.
- [2] Michael L Stein. *Interpolation of spatial data: some theory for kriging*. Springer Science & Business Media, 2012.
- [3] Peter Guttorp and Tilmann Gneiting. Studies in the history of probability and statistics xlix on the matern correlation family. *Biometrika*, 93(4):989–995, 2006.
- [4] Bertil Matérn. *Spatial variation*, volume 36. Springer Science & Business Media, 2013.
- [5] Larry C Andrews and Larry C Andrews. *Special functions of mathematics for engineers*. McGraw-Hill New York, 1992.
- [6] Budiman Minasny and Alex B McBratney. The matern function as a general model for soil variograms. *Geoderma*, 128(3-4):192–207, 2005.
- [7] Finn Lindgren, Håvard Rue, and Johan Lindström. An explicit link between gaussian fields and gaussian markov random fields: the stochastic partial differential equation approach. *Journal of the Royal Statistical Society: Series B (Statistical Methodology)*, 73(4):423–498, 2011.
- [8] Andrew TA Wood and Grace Chan. Simulation of stationary gaussian processes in $[0, 1]$ d. *Journal of computational and graphical statistics*, 3(4):409–432, 1994.
- [9] Claude R Dietrich and Garry N Newsam. Fast and exact simulation of stationary gaussian processes through circulant embedding of the covariance matrix. *SIAM Journal on Scientific Computing*, 18(4):1088–1107, 1997.
- [10] Johnathan M. Bardsley. *Computational Uncertainty Quantification for Inverse Problems*. SIAM, 2018.
- [11] Peter Whittle. On stationary processes in the plane. *Biometrika*, pages 434–449, 1954.
- [12] Lassi Roininen, Mark Girolami, Sari Lasanen, and Markku Markkanen. Hyperpriors for matern fields with applications in bayesian inversion. *arXiv preprint arXiv:1612.02989*, 2016.
- [13] Lassi Roininen, Janne MJ Huttunen, and Sari Lasanen. Whittle-matern priors for bayesian statistical inversion with applications in electrical impedance tomography. *Inverse Probl. Imaging*, 8(2):561–586, 2014.
- [14] Karla Monterrubio-Gómez, Lassi Roininen, Sara Wade, Theo Damoulas, and Mark Girolami. Posterior inference for sparse hierarchical non-stationary models. *arXiv preprint arXiv:1804.01431*, 2018.

- [15] Lassi Roininen, Petteri Piiroinen, Markku Lehtinen, et al. Constructing continuous stationary covariances as limits of the second-order stochastic difference equations. *Inverse problems and imaging*, 2013.
- [16] Havard Rue and Leonhard Held. *Gaussian Markov random fields: theory and applications*. CRC press, 2005.
- [17] Gabriel J Lord, Catherine E Powell, and Tony Shardlow. *An introduction to computational stochastic PDEs*. Number 50 in Cambridge texts in applied mathematics. Cambridge University Press, 2014.
- [18] John B Walsh. An introduction to stochastic partial differential equations. In *École d'Été de Probabilités de Saint Flour XIV-1984*, pages 265–439. Springer, 1986.
- [19] Sadri Hassani. Dirac delta function. In *Mathematical methods*, pages 139–170. Springer, 2009.
- [20] Mark S Gockenbach. *Partial differential equations: analytical and numerical methods*, volume 122. SIAM, 2005.
- [21] Ivar Stakgold and Michael J Holst. *Green's functions and boundary value problems*, volume 99. John Wiley & Sons, 2011.
- [22] Stanisław Saks. *Theory of the integral*. 1937.
- [23] Ian Naismith Sneddon. *Fourier transforms*. Courier Corporation, 1995.
- [24] Mateusz Kwaśnicki. Ten equivalent definitions of the fractional laplace operator. *Fractional Calculus and Applied Analysis*, 20(1):7–51, 2017.
- [25] Robert Piessens. The hankel transform. In Alexander D Poularikas, editor, *Transforms and Applications Handbook*, chapter 9. CRC Press, Boca Raton, FL, 2000.
- [26] Loukas Grafakos and Gerald Teschl. On fourier transforms of radial functions and distributions. *Journal of Fourier Analysis and Applications*, 19(1):167–179, 2013.
- [27] Harry Bateman. *Tables of integral transforms*. McGraw-Hill, 1954.
- [28] U Khristenko, L Scarabosio, P Swierczynski, E Ullmann, and B Wohlmuth. Analysis of boundary effects on pde-based sampling of whittle–matérn random fields. *SIAM/ASA Journal on Uncertainty Quantification*, 7(3):948–974, 2019.
- [29] Curtis R Vogel. *Computational methods for inverse problems*, volume 23. Siam, 2002.
- [30] Per Christian Hansen. *Rank-deficient and discrete ill-posed problems: numerical aspects of linear inversion*, volume 4. Siam, 2005.
- [31] Majid Jafari Khaledi and Firoozeh Rivaz. Empirical bayes spatial prediction using a monte carlo em algorithm. *Statistical Methods and Applications*, 18(1):35–47, 2009.
- [32] Christian Robert and George Casella. *Monte Carlo statistical methods*. Springer Science & Business Media, 2013.
- [33] Oliver Schabenberger and Carol A Gotway. *Statistical methods for spatial data analysis*. CRC press, 2017.
- [34] Noel Cressie. *Statistics for spatial data*. John Wiley & Sons, 2015.
- [35] W. Schwanghart. Experimental (Semi-) Variogram, 09 Jan 2013. MATLAB Central File Exchange. Retrieved 21 May 2018.
- [36] W. Schwanghart. variogramfit, 14 Oct 2010. MATLAB Central File Exchange. Retrieved 21 May 2018.
- [37] George Casella. An introduction to empirical bayes data analysis. *The American Statistician*, 39(2):83–87, 1985.
- [38] Dave Hale. Implementing an anisotropic and spatially varying matérn model covariance with smoothing filters. 2013.
- [39] Kathryn Anne Haskard. *An anisotropic Matern spatial covariance model: REML estimation and properties*. PhD thesis, University of Adelaide, 2007.
- [40] William G Jacoby. Loess:: a nonparametric, graphical tool for depicting relationships between variables. *Electoral Studies*, 19(4):577–613, 2000.
- [41] Gb11111. Arizona – the wave. Flickr. Retrieved 22 May 2019.
- [42] David S Watkins. *Fundamentals of matrix computations*, volume 64. John Wiley & Sons, 2004.